The SPECFIND V3.0 catalog of radio continuum cross-identifications and spectra: Reaching lower frequencies

Yelena Stein, Bernd Vollmer, Thomas Boch, Gilles Landais, Patricia Vannier, Marianne Brouty, Mark G. Allen, Sébastien Derriere, Pierre Ocvirk

Astronomy & Astrophysics manuscript no. output
November 6, 2021

The SPECFIND V3.0 catalog of radio continuum cross-identifications and spectra – Reaching lower frequencies

Y. Stein, B. Vollmer, T. Boch, G. Landais, P. Vannier, M. Brouty, M. G. Allen, S. Derriere, and P. Ocvirk

Observatoire astronomique de Strasbourg, Université de Strasbourg, CNRS, UMR 7550, 11 rue de l'Université, 67000 Strasbourg, France; e-mail: bernd.vollmer@astro.unistra.fr

Received October 12, 2020

ABSTRACT

Context. Many radio continuum catalogs with different sensitivity limits and spatial resolutions are published via the VizieR database at the Centre de Données astronomiques de Strasbourg (CDS). The diversity of spatial resolutions of different catalogs makes the cross-identification of different flux density measurements of individual sources complex. The SPECFIND tool is able to handle radio surveys at different frequencies from different instruments with different resolutions.

Aims. Since the former version of the SPECFIND catalog was released ten years ago, hundreds of new radio continuum catalogs have been published. We upgraded the SPECFIND tool to reach a wider frequency range, especially the lower-frequency radio regime, as well as to have better spatial sky coverage.

Methods. We adapted selection criteria and applied them to all of the radio catalogs listed in the VizieR database to define a final sample of new catalogs. We unified the new catalogs and implemented them in the SPECFIND tool. The new SPECFIND V3.0 radio cross-identification catalog was constructed using 204 input tables from 160 VizieR radio continuum catalogs to cross-identify flux density measurements of individual sources and fit their spectral slopes. We discuss the frequency and sky coverage of all processed catalogs and compare the results to the previous version. Furthermore, we present and investigate peaked spectrum (PS) sources with spectral breaks around 1.4 GHz and 325 MHz.

Results. By increasing the number of input catalog tables that were implemented in SPECFIND from 115 to 204 (89 new catalog tables and two updates), we improved the number of resulting spectra from ∼107 500 to ∼340 000 and increased the number of cross-identified sources from ∼600 000 to ∼1.6 million. The final SPECFIND V3.0 catalog is publicly available via VizieR. By applying SPECFIND to two subsamples of the catalogs with frequency cuts at 325 MHz and 1.4 GHz, spectral break and PS source candidates could be identified. We encourage follow-up observations of these candidates to confirm their nature because the population we identify has a relatively low reliability.

Conclusions. The SPECFIND V3.0 catalog is a very useful resource and a powerful open access tool, reachable via VizieR. By tripling the resulting spectra and including many radio continuum surveys from the last 50 years, we provide a significantly extended catalog of cross-identified radio continuum sources. Furthermore, the SIMBAD database will be updated using the SPECFIND V3.0 catalog and will contain more radio continuum data, serving the needs of future projects.

Key words. Virtual observatory tools, Catalogs, Radio continuum: general, Methods: data analysis

1. Introduction

Within the last few decades, a variety of radio continuum observations of major parts of the sky have been conducted, leading to many different radio continuum source catalogs. The observations are usually undertaken with different interferometric arrays or single dish telescopes, leading to a huge range of resulting resolutions and sensitivities as well as pointing precisions. The SPECFIND tool (Vollmer et al. 2005a), with applications and later versions (Vollmer et al. 2005b, 2008, 2010), was introduced to handle these diverse radio catalogs. It uses catalogs from the VizieR database[1] (Ochsenbein et al. 2000) of the Centre de Données astronomiques de Strasbourg (CDS) to cross-identify radio sources of the different catalogs and produces spectral energy distributions (SEDs) over a large frequency range in the radio continuum regime. Since the release of the SPECFIND V2.0 catalog, several of the recently published radio continuum catalogs have significantly improved the sky coverage, especially in the low-frequency regime for example, the TIFR GMRT Sky Survey Alternative Data Release (TGSSADR, Intema et al. 2017a), the GaLactic and Extragalactic All-sky MWA survey (GLEAM, Hurley-Walker et al. 2017a), or the LOFAR Two-metre Sky Survey DR1 (LOTSS DR1, Shimwell et al. 2019a). Therefore, we upgraded SPECFIND to include these along with other VizieR catalog tables with more than 150 entries. This has nearly doubled the number of ingested catalog tables and increased the number of input sources by a factor of 60, with more than 5 million input sources in SPECFIND V3.0.

The radiation in the radio continuum is dominated by emission originating from relativistic cosmic ray electrons (CREs) gyrating around magnetic field lines and, while doing so, emitting nonthermal synchrotron emission perpendicular to the magnetic field orientation. An ensemble of relativistic electrons with a wide energy range of individual energy distributions following a power-law relation (see, e.g., Pacholczyk & Swihart 1970; Condon 1992) leads to the observed SED of synchrotron radiation following a power law, where the observed flux density S_ν at frequency ν is proportional to ν^α with the spectral index α. If considered in log-log space (log(frequency) vs. log(intensity)), the spectral index α is the slope of the linear relation, commonly

[1] http://vizier.u-strasbg.fr/viz-bin/VizieR

$\alpha \sim -0.7$ (Condon 1992). A contribution of thermal emission is expected depending on the frequency (e.g., 20% at 6 cm wavelength, Condon 1992) which has a flat spectral slope of $\alpha = -0.1$ in the log-log space. The majority of radio continuum sources show a resulting linear slope in the radio regime. Therefore, the SPECFIND tool uses a linear fit for the spectra. Nevertheless, spectral flattening or inversion can occur toward lower frequencies due to synchrotron self-absorption or free-free absorption as well as spectral steepening toward higher frequencies due to the aging of CREs (see, e.g., O'Dea 1998).

Gigahertz-peaked spectrum (GPS), high-frequency peaked (HFP), or compact steep spectrum (CSS) sources are powerful radio continuum sources showing inverted spectra with a positive spectral slope in the megahertz regime up to a turnover frequency with a negative spectral index toward higher frequencies (see the reviews O'Dea 1998; O'Dea & Saikia 2021). The spectral break of GPS sources can be observed in different sources, such as quasars, active galactic nuclei or galaxies. Variable GPS sources are often connected to blazars (e.g., Tinti et al. 2005; Ross et al. 2021). A source is classified differently, based on the turnover frequency and the turnover curvature, as well as a spectral index of $\alpha \geq 0.5$ below the associated turnover frequency. While CSS sources are the least compact (up to ~20 kpc) in comparison to the other two, they show their turnover frequency in the megahertz regime $\leq$ 500 MHz. GPS sources have turnover frequencies in the gigahertz regime of ~0.5 – 5 GHz. They are more compact (~1 kpc) than CSS sources. HFP sources are defined to have turnover frequencies $\geq$ 5 GHz and are very compact ($\leq$1 kpc). These three different types of sources are referred to as peaked spectrum (PS) sources (O'Dea & Saikia 2021) and could represent an age sequence, where HFP sources are younger stages of GPS sources, which ultimately transform into CSS sources and then even into larger and more powerful radio sources. This aging scenario is concluded from observations of turnover frequencies and linear sizes of different objects (e.g., Fanti et al. 1990). The steepening of the spectrum toward lower frequencies can be explained by two different mechanisms: via synchrotron self-absorption or free-free absorption (e.g., Snellen et al. 1998).

In this new SPECFIND upgrade, we are able to detect sources that peak at around 1.4 GHz and 325 MHz. While belonging to the overall class of PS sources, we call the sources with turnover frequencies around 1.4 GHz satisfying $\alpha \geq 0.5$ below the turnover frequency GPS source candidates. We call sources with turnover frequencies around 325 MHz megahertz-peaked spectrum (MPS) source candidates. Furthermore, we classify a sample of PS sources that have $\alpha \geq 0.3$ below the turnover frequency and $\alpha \leq$ -0.3 above the turnover frequency as concave source candidates.

The paper is organized as follows. In Section 2 we provide basic explanations of how the SPECFIND tool works. Section 3 describes the upgrade in terms of software and the selection criteria for the newly added radio continuum catalog tables. In Section 4 the results are presented and compared to the previous version of the SPECFIND catalog. We describe an application of the SPECFIND tool to find PS sources and provide example sources that have a clear spectral break either around 325 MHz (MPS source candidates) or around 1.4 GHz (GPS sources candidates) in Section 5. In Section 6 we explain how to access the public SPECFIND V3.0 catalog via VizieR as well as the structure of the published tables. The summary and conclusions are provided in Section 7.

2. The SPECFIND tool

Generally, the SPECFIND tool cross-identifies flux density measurements of sources from radio continuum catalog tables at different frequencies from the VizieR database and fits a single power law (linear spectral slope in log-log space) to the cross-identified flux density measurements. In principle, SPECFIND allows for one break in the spectrum, which means it can fit two different slopes to the radio continuum spectrum. However, since the SPECFIND algorithm is optimized for the robust fitting of a single spectral slope, spectral breaks are rarely fit to the data (see Fig. 10 in Vollmer et al. 2010). Similarly, any curvature in a spectrum due to flattening toward lower frequencies (synchrotron self-absorption or free-free absorption) or steepening toward higher frequencies (CRE aging) is only very rarely fit by the SPECFIND algorithm. Instead, a single spectral index is determined for the part of the spectrum with the highest frequency coverage above or below the break frequency. For SPECFIND V3.0 we undertook a more detailed analysis of the cases that show a spectral break with different spectral indices on the lower and the higher-frequency part of our catalog sample (Section 5).

In the context of the SPECFIND cross-identification of flux density measurements of radio continuum sources the following terms are important. The different VizieR *catalogs* can contain one or more tables. A *table* in VizieR belongs to a catalog. Therefore, we often use the term "catalog table." Relevant tables contain at least sky coordinates and a radio continuum flux density. Additional parameters are the error on flux density, source size, and position angle. We produced SPECFIND input tables from these tables. If flux density measurements at different frequencies are present in a VizieR table, it is split into different SPECFIND input tables. Cross-identified flux density measurements from different tables belong to one *object* in the SPECFIND catalog. Each object contains at least three flux density measurements observed at independent frequencies. Every object has one associated *spectrum* that is the collection of the associated flux density measurements.

SPECFIND uses its own requirements for the catalog entries: coordinates in J2000 and their associated uncertainties; flux density and its associated uncertainty; major and minor axis and position angle; source name. More details on these SPECFIND catalogs and how we unified and ingested them will be explained in Section 3.3.

SPECFIND is a hierarchical code. It classifies a flux density measurement *j* as parent, sibling or child with respect to a given flux density measurement *i* at different stages where stage 2 and 3 are refinements of stage 1.

stage 1: depending on proximity criteria:

- parent: flux density measurement *j* has a larger extent or was observed with a lower angular resolution than flux density measurement *i*,
- sibling: flux density measurement *j* has a comparable extent or was observed with a comparable angular resolution (within 25%) to that of flux density measurement *i*,
- child: flux density measurement *j* has a smaller extent or was observed with a higher angular resolution than flux density measurement *i*.

stage 2: depending on flux densities at the same frequency:

- parent: flux density measurement *j* has a larger extent or resolution and has a larger flux density than flux density measurement *i*,

- sibling: flux density measurement j has a comparable extent or resolution and has the same flux density within the errors as flux density measurement i,
- child: flux density measurement j has a smaller extent or resolution and a smaller flux density than flux density measurement i.

stage 3: depending on flux densities at different frequencies, based on the expected radio spectral index:

- parent: flux density measurement j has a larger flux density than expected from the radio spectrum that includes flux density measurement i,
- sibling: flux density measurement j fits into the radio spectrum that includes flux density measurement i,
- child: flux density measurement j has a smaller flux density than expected from the radio spectrum that includes flux density measurement i.

At the end of this procedure flux density measurement i and its siblings are considered the same flux density measurement. Once the cross-identification based on the flux density measurements at the same frequency is done, the family dependences are verified, which means for a given flux density measurement cross-checks are performed. These checks are performed for all SPECFIND catalog entries:

- If flux density measurement j is a sibling of flux density measurement i, then flux density measurement i must also be a sibling of flux density measurement j.
- If flux density measurement j is a child of flux density measurement i, flux density measurement i must be a parent of flux density measurement j.
- If flux density measurement j is a parent of flux density measurement i, flux density measurement i must be a child of flux density measurement j.

The heart of SPECFIND is the spectrum-finding algorithm. It uses the method of the least absolute deviation to make a linear fit in the $\log \nu$–$\log S_\nu$ plane. This method is more robust against outlying points in a spectrum than a standard least-squares deviation (χ^2) fit (see Press et al. 2002). For this algorithm, the best way to find a maximum number of spectra without a too high risk of spectral misidentifications is to set the flux density errors of all flux density measurements that are smaller than 30 % of their flux density to 30 %. In this way all catalogs have approximately the same relative error. This scaling was found heuristically by Vollmer et al. (2005) and (2010). It led to a high number of cross-identifications with a relatively low number of misidentifications. Moreover, these relatively large errors can compensate for some flux density measurement variability and calibration offsets, for example, known for the WENSS (Hardcastle et al. 2016).

The structure of the spectrum-finding algorithm is explained the following. For a given set of flux density measurements for which all family relations were determined, their flux measurements at different frequencies are grouped together into an array and sorted by frequency. If the number of different frequencies is greater than two, the spectrum-finding algorithm passes through the following steps, where spectra are fitted to all SPECFIND catalog entries individually:

1. A least absolute deviation fit in the $\log S_\nu - \log \nu$ plane is performed:

$$\log S_\nu = \alpha \log \nu + \gamma \; ; \tag{1}$$

2. If the spectrum is determined more than once, the number of flux density measurements that fit into the spectrum is checked. If it decreases, the old fit parameters are used;
3. A check if flux density measurements fit into the spectrum is performed; if all flux density measurements fit, the algorithm goes to step 6.;
4. If there are two flux density measurements of the same frequency, the one with the largest deviation from the fit is flagged and removed;
5. If all flux density measurements have different frequencies the flux density measurement with the largest deviation from the fit is flagged and removed, the algorithm goes to step 1.;
6. If there are more than two independent points left and if the ratio between the largest and the smallest frequency interval is greater than 0.02, the final fit is performed;
7. The algorithm goes to step 1 and performs a second run with fir parameters of $\alpha = -0.9$ and $\gamma = \log S_\nu - \alpha \log \nu$ during the first $N-4$ steps of the loop, where N is the initial number of points in the spectrum (– 0.9 is the mean spectral index of all radio flux density measurements);
8. If the number of fitted points with fixed γ and α exceeds that of the initial fitting procedure, this spectrum is accepted; otherwise, the spectrum of the first fitting procedure is accepted.

In order to avoid using points that are too close to one another in frequency, and therefore not independent, the frequency intervals between the different points of the spectrum are checked. The routine calculates the frequency intervals and determines the ratio between the second largest and the largest frequency interval. If this ratio is smaller than 0.02, the spectrum is rejected.

Then, in order to avoid ambiguous radio flux density measurements of a given frequency, which are attributed to two distinct physical objects, the "center of mass" coordinates are calculated for both objects, where the inverse of the survey resolution is used for the "mass." The ambiguous flux density measurement is then attributed solely to the object whose "center of mass" position is nearest to the flux density measurement position.

A completeness and uniqueness check for all spectra ensures that if a flux density measurement j fits the spectrum determined for flux density measurement i (where flux density measurement i is included), then flux density measurement i also appears in the spectrum of flux density measurement j. In this way it is ensured that a radio flux density measurement belongs to only one single physical object.

3. SPECFIND V3.0

SPECFIND V3.0 contains minor changes in terms of software. With the addition of 91 catalog tables the number of input catalog tables was almost doubled with respect to SPECFIND V2.0.

3.1. Software

The software was modified to improve the spatial cross-identification via a revised proximity criterion: if the proximity criterion is not fulfilled by one source, we now allow the exclusion of this spectral point, whereas in the previous version the entire associated object was removed. This increased the number of resulting spectra by 3%, which corresponds to several thousand spectra.

3.2. Adding new catalogs

In order to add relevant catalogs, we searched in the VizieR database for catalogs containing radio data with source posi-

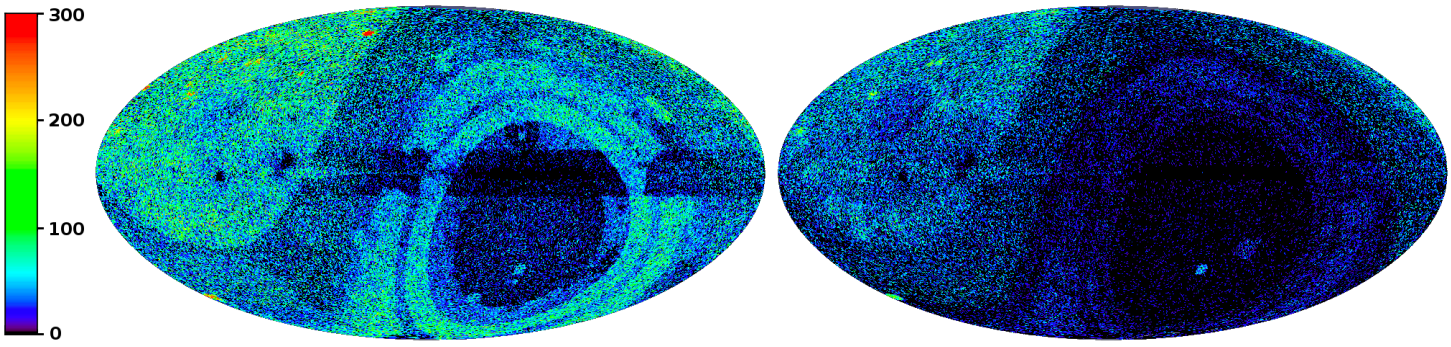

Fig. 1: Comparison of the sky coverage density map of SPECFIND V3.0 (left) and SPECFIND V2.0 (right). The color represents the number of sources per healpix size of 0.2 deg^2.

tions available in the table. This search can be done directly in VizieR via the Unified Content Descriptor (UCD) search capability. The UCDs are an International Virtual Observatory Alliance (IVOA[2]) standardized (Derriere et al. 2004; Martinez et al. 2018) description of astronomical quantities. The basic UCD search can be accessed on the VizieR web page. The other way to obtain catalogs with certain UCD criteria is via the TABFIND services, a Structured Query Language (SQL) search by the Tool for OPerations on Catalogs And Tables (TOPCAT[3], Taylor (2011)). In order to deal with the resulting tables and to apply additional selection criteria we used TOPCAT. We obtained all radio data catalogs with positional and flux information included (UCD:"(pos.*)&(phot.flux*;em.radio*"). The VizieR database holds more than 1200 catalogs containing radio data[4]. Some of these catalogs consist of several tables, which leads to approximately 2400 tables containing radio data or being connected to radio data. To find useful catalogs for the SPECFIND tool, we first chose the number of records that is the number of rows within each table to be larger or equal to 150.

We ended up with approximately 1000 tables to investigate manually. We discarded all tables not related to radio continuum observations of point sources such as, all tables containing neutral hydrogen (HI) surveys or description tables containing no radio continuum data at all. Applying further criteria (radio continuum data between a few MHz and up to 31 GHz and no time series) led to roughly 110 tables. We discarded many deep field catalogs (e.g., the Swire field and the COSMOS field) because we need at least a few square degrees sky coverage within one table to have an impact on the SPECFIND results. In the last step we had to discard catalogs with large beams (> 30 arcmin) since the cross matching fails if the beam is too large. In the following we summarize the selection criteria for our radio continuum catalogs:

- at least 150 flux density measurements in the table
- radio continuum data between a few MHz and up to 31 GHz
- no time series
- minimal flux density $\geq$ 0.01 mJy to avoid deep fields (like, e.g., the Hubble Deep Field)
- sky coverage $\geq$ 2 deg^2
- beam sizes $\leq$ 30 arcmin.

These criteria led to 91 new catalog tables[5]. Two catalog tables were replaced by a new version of the same data: VLA Low-frequency Sky Survey Redux (VLSSr, Lane et al. 2014) and Faint Images of the Radio Sky at Twenty centimeters Version 2014 (FIRST14, Helfand et al. 2015). 89 catalog tables were added to the existing 115 ones of version 2.0. This resulted in 204 catalog tables originating from 160 VizieR catalogs that were included in SPECFIND V3.0 (Table A.1).

3.3. Unification

The VizieR radio catalogs have been published by a wide range of authors, with a multitude of different original purposes. As such, these catalogs have a diverse range of ways of expressing the properties of radio sources. VizieR provides a high level of homogenization so that they comply with the CDS standard for catalogs. To process the radio catalogs for SPECFIND we take this process a step further to provide a higher level of interoperability of these catalogs. In particular by further unifying the catalogs for the SPECFIND tool (e.g., taking into account specific properties of radio sources).

This unification procedure was made efficient by using an ingestion and unification tool, developed at CDS. For more details on that and the entire procedure of unification of the different radio tables see Vollmer et al. (2010). The information of the observational characteristics was gathered for each catalog (mostly by manually searching in the associated paper). This included the beam size of the observations in arcsec, the minimum flux density of the observations (i.e., faintest detected source in the respective survey) in mJy and the flux density measurement error of the observations (if not mentioned, 15% was assumed). In the appendix Table A.1 we summarize the information about the observing frequency, the beam size, the minimum flux density, the number of sources, the percentage of the catalog that was processed by the SPECFIND tool and the reference with its associated VizieR catalog name.

Each ingested catalog table includes the general information (Number of sources in the table, frequency and beam size of the observations) and the source information for each source (coordinates RA and Dec, flux density and its error in mJy, source size in units of the beam size, its position angle and the source name). The source name was either used directly from the source names in the VizieR table or was newly assigned. When no acronym was provided by the authors of a catalog, a unique acronym was created directly linked to the corresponding publication and defined in coordination with the Dictionary of Nomenclature[6]. These acronyms are based on the initials of the first three authors

[2] https://ivoa.net/
[3] http://www.starlink.ac.uk/topcat
[4] as of May 2020
[5] Due to technical problems, the AT20G catalog (Murphy et al. 2010) was not included in the sample.
[6] http://cds.u-strasbg.fr/cgi-bin/Dic

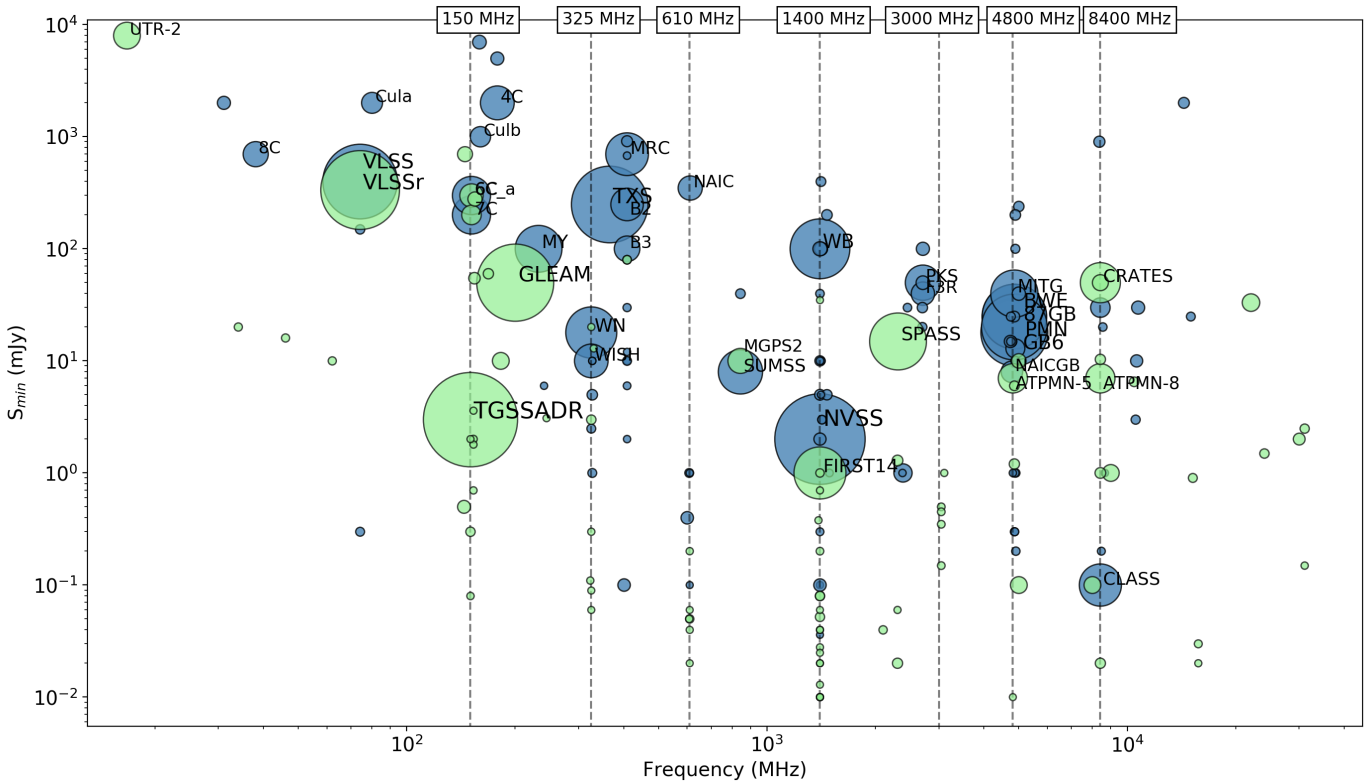

Fig. 2: Minimal flux density (S_{min}) vs. frequency of the 204 catalog tables used in SPECFIND V3.0. The size of the circles represent the sky coverage of the catalogs. Labeled catalogs have more than 210 deg^2. Green shaded catalogs were added in version 3.0, blue shaded catalogs were already included in version 2.0.

followed by the year of publication. Since SPECFIND needs to distinguish between sources observed at different frequencies within the same VizieR table, a letter or the frequency has been added to the acronym when necessary.

3.4. Compability to V2.0

To ensure that SPECFIND version 3.0 and 2.0 are compatible we used the SPECFIND Comparison tool, which was developed at CDS (see Vollmer et al. 2010, for further explanation). This tool is able to compare the different output spectra from both versions. It finds differences in cross-identified flux density measurements between the two versions and shows this next to each other with a view of the corresponding spectrum. It is possible to merge both cross-identification spectra or chose one spectrum. Secondly it also enables us to add the sources from V2.0 which were originally not included in V3.0. In this tool, more than 7000 spectra were inspected by hand due to either different or missing spectra in version 3.0. In this way, we created a consistent final SPECFIND V3.0 catalog. The final catalog containing the spectra of the different sources and the spectral slopes was ingested into the VizieR database ("spectra" table). Additionally, all rejected spectra ("waste" table) and the catalog list ("beam" table) were added to the VizieR database (see Sect. 6).

4. Results

In total, SPECFIND V3.0 found 339592 objects with corresponding radio continuum spectra by processing 204 input catalog tables (see Table A.1). These objects have at least three independent frequency points, which means data points coming from three different SPECFIND input catalog tables with radio continuum data observed at different frequency bands. The total number of cross-identified sources is ∼1.6 million.

4.1. Comparison to SPECFIND V2.0

In comparison to the 107500 resulting spectra of SPECFIND V2.0, the number of output spectra was increased by more than a factor of three. In Figure 1 the sky coverage density maps of SPECFIND version 2.0 and 3.0 are shown next to each other. This shows the major improvement in the sky coverage that has been achieved in version 3.0.

4.2. Frequency coverage and minimum flux density

Figure 2 shows a plot of the minimum flux density against the frequency of the 204 catalog tables. Each catalog table is represented by one circle and its size indicates the sky coverage of the catalog. Green shaded catalog tables were added to SPECFIND V3.0, blue shaded catalog tables were already included in version 2.0. Only catalog tables with a sky coverage larger than 200 deg^2 are labeled. Roughly half of all catalog tables contain data at frequencies above or equal to 1.4 GHz. There are concentrations of catalogs at certain observed frequencies, marked in Fig. 2. These are the radio continuum bands at 150 MHz, 325 MHz, 610 MHz, 1.4 GHz (L-band), 3 GHz (S-band), 4.8 GHz (C-band) and 8.4 GHz (X-band). See also to Appendix Figure A.1 for a similar plot, where the circle size represents the number of sources in each catalog table. From these two figures, it becomes clear that the catalogs TGSSADR as well as GLEAM and LOTSSDR1 have a major impact on the result-

ing increased number of spectra. While all three contribute in the low-frequency radio continuum regime, the GLEAM catalog additionally covers the southern hemisphere, where fewer catalogs are available. For GLEAM, we use the mean spectral point to not give an overweight to this survey.

As a sanity check, we compared the two updated catalogs, VLSSr and FIRST14, with their former versions within SPECFIND V3.0. By replacing the VLSS (Cohen et al. 2007) with the VLSSr catalog, the number of VLSS sources was increased from ∼68 000 to ∼92 000. By replacing the FIRST (White et al. 1997) with the FIRST14 catalog, the number of FIRST sources was increased from ∼810 000 to ∼946 000. SPECFIND V3.0 was able to process ∼67 000 VLSSr sources, in comparison to ∼53 600 VLSS sources. The same trend is visible for the FIRST catalog, which was updated to FIRST14. We were able to cross-identify ∼59 700 FIRST14 sources, in comparison to ∼53 800 FIRST sources. In summary, we found higher numbers of cross-identified sources in the new catalogs.

4.3. Spectral indices

The spectral index distribution (Fig. 3) shows a peak around α = -0.9, which is consistent with the former SPECFIND versions. The median spectral index is $\alpha = -0.75$ with a semi-inter-quartile-range (SIQR) of 0.28. The median and SIQR agree with other measurements: the cross-identification of VLSSr and NVSS led to $\alpha = -0.82$ with an SIQR of 0.11 (Lane et al. 2014), that of SUMSS and NVSS to a median spectral index of −0.83 (Mauch et al. 2003). The median spectral index within the GLEAM band is about −0.8 (Hurley-Walker et al. 2017b). The distribution shows a tail to positive spectral indices, which is caused by sources with low flux densities at 325 MHz (Fig. 4). Since this tail is not present in the VLSSr-NVSS spectral index distribution, it is most probably caused by our selection bias (see Fig. 2): The WENSS survey together with the relatively shallow 5 GHz surveys (GB6, 87GB, MITG, BWE, PMN) and the deep TGSSADR survey favors the detection of sources with positive spectral indices. Additionally, we inspected the tail and discarded sources by hand with spectral indices > 2 showing source confusion.

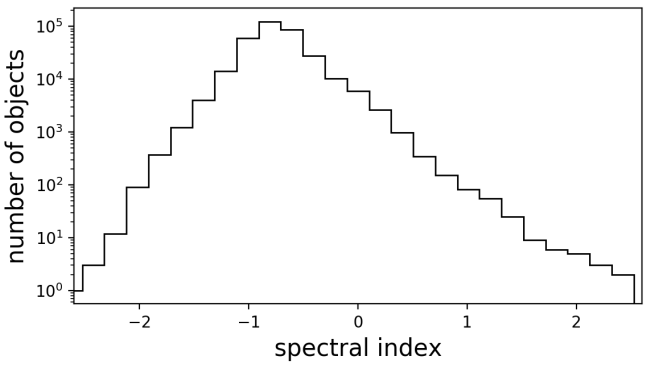

Fig. 3: Histogram of the spectral index distribution for all resulting spectra/objects of SPECFIND V3.0.

Figure 4 represents the distribution of the spectral indices as a function of the measured Westerbork Northern Sky Survey (WENSS) flux density at 325 MHz. If not available, the flux density of another catalog at 325 MHz was used. If no flux density measurement existed at that frequency, we calculated the value by interpolating the flux density at 325 MHz from the spectral fit. The general appearance is consistent with that of V2.0. The majority of the objects (dark region) have spectral indices of ∼ −0.7 irrespective of the flux densities at 325 MHz. This spectral slope is expected for synchrotron emission.

There are two main features that deviate from the dark region with a constant spectral index: (i) a wing toward the top-left of the figure with low flux densities (< 300 mJy) and flat spectral indices (> −0.3) and (ii) a bump toward the bottom of the figure with low flux densities and steep spectral indices (< −1.5). Systematic shifts in the flux density scales of some surveys are expected to lead to a spectral index offset of about 0.2. For example, a downscaling of the WENSS flux by a factor of 0.8 as stated by Hardcastle et al. (2016) flattens a spectrum from a spectral index of -0.70 [−0.83] to -0.55 [−0.7]. This offset is not large enough to explain the SI deviations from the mean in the wing and the bump. We inspected sources in both regions by eye using the Aladin lite and the VizieR photometric viewer. There are many objects in the wing (S_{325} < 100 mJy, SI> 0), which include WENSS/WISH and NVSS flux densities together with a flux density at a lower frequency (e.g., TGSSADR), or at higher frequency (e.g., PMN). We did not find a significant number of objects where source confusion was suspected. The objects in the bump mostly contain NVSS and WENSS/WISH sources together with sources at frequencies below 325 MHz. As before, we did not find obvious problems with these objects. We therefore conclude that the deviations from the mean SI are caused by flux density scale issues that are signal-to-noise dependent and the minimal observed flux densities or sensitivities of the different catalogs (Fig. 2). Drawing lines through S_{325} = 100 mJy with spectral indices > 0 and < −1.5 gives insight into which catalogs are expected to be involved in the objects in the wing and bump.

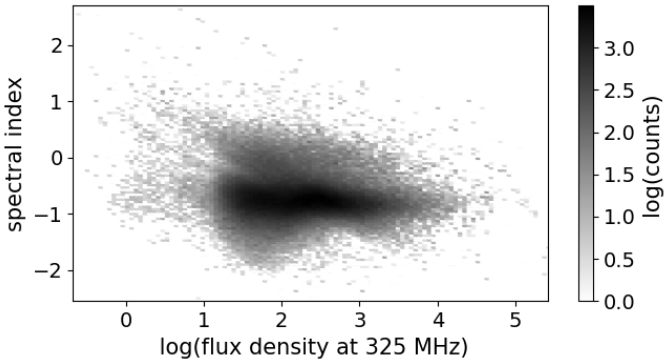

Fig. 4: Spectral index as a function of the flux density at 325 MHz. For spectra with no corresponding measurement at 325 MHz, the interpolated value of the spectral fit was calculated.

4.4. Number of sources

In Figure 5 we present the distribution of the number of sources, which means the distribution of how many independent frequency points are contained in an object/spectrum. The distribution begins at a number of three sources (frequencies) since this is the minimum number to produce an output spectrum with the SPECFIND tool. There is a slight excess of the number of objects containing three or four sources, as was the case for SPECFIND V2.0 (see Vollmer et al. 2010). In SPECFIND V3.0

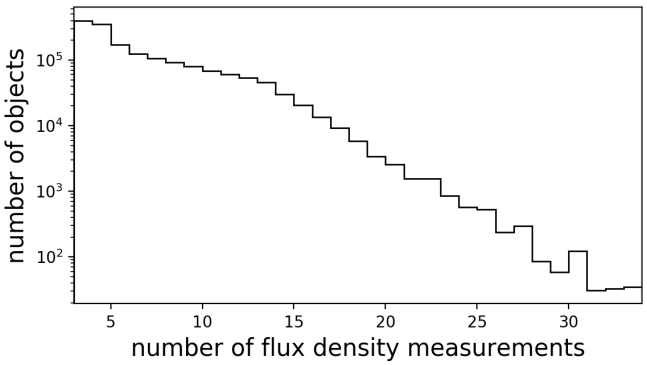

Fig. 5: Histogram of the spectra (or objects) with a given number of flux density measurements of SPECFIND V3.0.

the maximum number of sources in a spectrum is 34, compared to 30 SPECFIND V2.0.

4.5. Complex radio sources

The SPECFIND tool finds mainly individual radio continuum point sources. However, sources in radio continuum catalogs can occur not only as simple point sources, but with diverse appearances as extended sources, complex or double sources. Additionally, there can be source confusion, with two or more physically unrelated sources located within a beam.

During the consistency check between versions 2.0 and 3.0, we inspected a subsample of 7000 complex sources by eye. While most of these sources are separated into different final spectra, we find a ∼6% contamination of double radio lobes or confused sources in crowded fields, which are assigned to one corresponding spectrum including all sub-sources. In most cases, this is apparent in the spectrum by parallel or intersecting lines of different spectral indices. Therefore, we advise the user to always inspect the data in Aladin Lite, which is available within the VizieR catalog of SPECFIND V3.0 (see Section 6).

The different radio continuum surveys have different resulting beams. Therefore, with a small beam (high resolution), extended sources are resolved, whereas with a large beam (low resolution), source confusion is an issue, if the source separation is smaller than the beam size. The SPECFIND tool is able to fit spectra to most of these sources (see Sect. 5 and appendix for further discussions on limitations). Nevertheless, the more complex a source is and the closer two or more different sources are, the harder is it to cross-identify the correct sources due to the different beams. In order to evaluate the results of SPECFIND V3.0, we revisited some of the sources shown in Vollmer et al. (2010) and compare the resulting spectra. These are shown in Fig. 6 to 8.

Most of the point sources and double sources that have been compared, show the same resulting spectra in the two versions (for example Fig. 6). For the three close sources around WN B2228.2+5940A (Fig. 7), we find a merged spectrum in SPECFIND V2.0 that includes two of the three sources. In SPECFIND V3.0 two individual spectra are found for two of the three sources with the third source that have no corresponding spectrum. In each version of the SPECFIND catalog, the SPECFIND tool missed one spectrum of the three sources. We find a tendency that the merged sources of version 2.0 are well separated in V3.0. In the case of the complex source WN B2040.8+4246 (Fig 8), version 3.0 shows a cleaner result, because the points, which do not cover the full source and thus show too little flux densities, are excluded.

4.6. Examples of new radio continuum source spectra

In Fig. 9 we show three examples from the ∼232 500 new spectra of SPECFIND V3.0 that are not included in V2.0. As is visible in the histogram (Fig. 5), most spectra include three to five sources. Many of these spectra include sources of the NRAO VLA Sky Survey (NVSS, Condon et al. 1998) and TGSSADR due to the large sky coverage of both catalogs. One example of this kind of spectra is shown on the left of Fig. 9 for the source NVSS J135722+732125. Another new spectrum of source NVSS J171701+191740 is shown in the middle of Fig. 9. With ten associated frequency points, it shows a spectral break at around 5 GHz. In the spectral break analysis of our entire sample which is presented in Section 5, we show that we are mostly sensitive to spectral breaks below 1.9 GHz and thus this source is not included in our sample of spectral break sources. A spectrum of the double source NVSS J123317+670808 is presented on the right of Fig. 9. The twenty associated frequency points show two distinct spectral slopes, which represent two different sources.

5. Data analysis - Peaked spectrum sources

The upgrades of SPECFIND V3.0 described above led to a well-sampled frequency coverage over the radio spectrum and thus enabled us to investigate possible spectral breaks of PS sources. However, we were only very rarely able to detect these sources using the SPECFIND tool in its classical design where a single power law is fit to the data within the full frequency range. Since the SPECFIND tool tries to include as many sources as possible in the fit, spectral break sources often end up either losing the peak spectral point(s) or one side of the spectrum, either the low- or the high-frequency part. Thus, these source were mostly unrevealed.

To identify spectral break source candidates, we divided the sample of catalog tables into two frequency parts to fit individual spectral slopes to each side of the turnover frequency. We created two catalog subsamples, one subsample below and one subsample above a selected frequency cut. The corresponding frequency of the cut is included in both subsamples to allow for cross-identification. The SPECFIND tool was applied on these subsamples individually. The two complementary spectra of the two subsamples were then combined into one object if they contained the same flux density measurement at the common frequency. In a second step, the fitted spectral slopes of the two subsamples were compared for each object. This procedure was done for two different frequency cuts to find GPS source candidates around 1.4 GHz and to find MPS source candidates around 325 MHz. The comparison of the spectral slope between the high and low-frequency part of an object led to three different criteria to identify (1) spectral break sources (sb), (2) concave spectrum sources (conc), (3) GPS and MPS sources with the criterion of O'Dea (1998). The spectral slope of the subsample of lower or equal frequencies in comparison to the frequency cut is $\alpha_{\rm low}$, the spectral slope of the subsample with frequencies higher than or equal to the frequency cut is $\alpha_{\rm high}$. The different criteria are defined as:

(1) spectral break sources (sb): $|\ \alpha_{\rm low} - \alpha_{\rm high}\ | \geq 0.3$
(2) concave spectrum sources (conc): $\alpha_{\rm low} \geq 0.3$ and $\alpha_{\rm high} \leq -0.3$
(3) GPS and MPS sources (gps/mps): $\alpha_{\rm low} \geq 0.5$ and $\alpha_{\rm high} \leq -0.3$

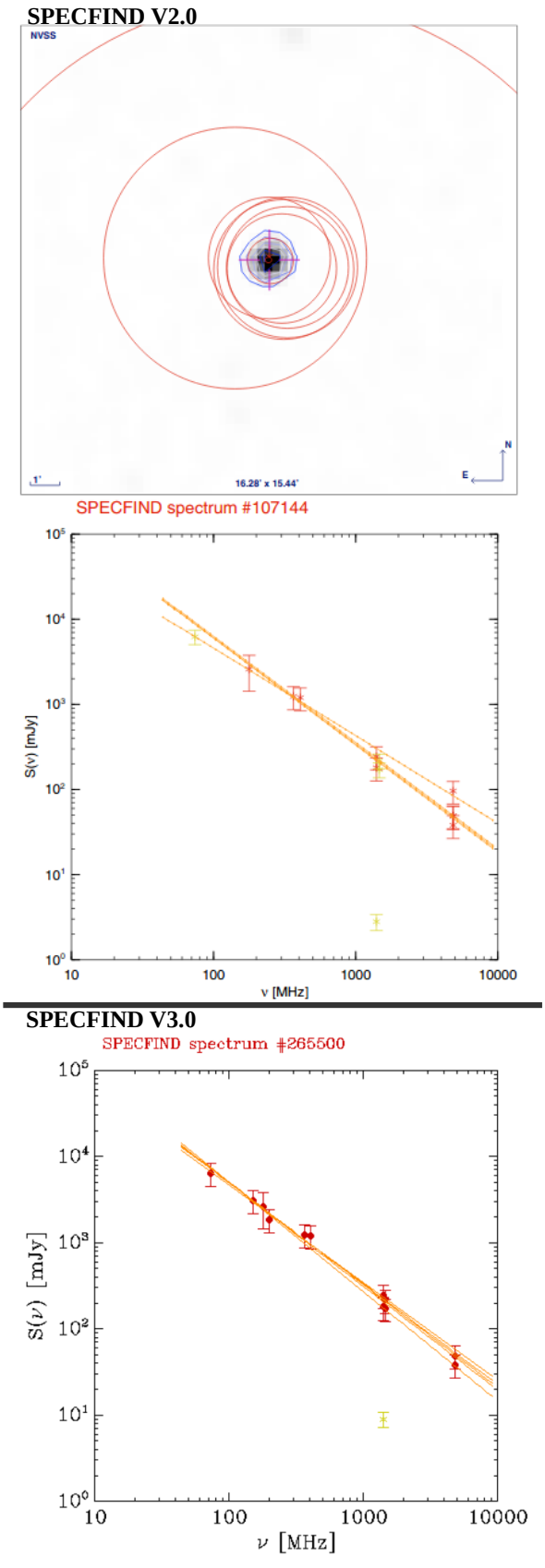

Fig. 6: Comparison of the resulting spectra of source TXS 2112+158 for SPECFIND V2.0 and V3.0. Top: NVSS grayscale and blue contours. Red circles are the beams of the catalogs included in the spectrum. Middle: SPECFIND V2.0 spectral fit. Bottom: SPECFIND V3.0 spectral fit. Yellowish green crosses have been discarded during the fitting process. Both versions show similar spectra with more sources included in version 3.

Finally, we discarded convex sources from the spectral break sample to avoid false positive detections due to confusion. Convex PS sources fulfill criterion (1) for spectral break sources and have $\alpha_{\rm low} < \alpha_{\rm high}$. It turned out that most of the convex sources in our sample were composed of two distinct sources with $\alpha_1 < \alpha_2$. The flux densities of source 1 dominate at low frequencies, those of source 2 dominate at high frequencies. Confusion of two sources with different constant spectral indices within the same resolution element most frequently leads to a convex spectrum.

For objects with concave spectra source confusion can occur because of different spatial resolutions at low and high frequencies: by inspecting the NVSS maps of 100 objects with a spectral break at 325 MHz and a concave spectrum by eye we found 16 resolved sources. The majority of these sources are elongated with major axes between 1.5′ and 3′. Sometimes, the objects contain several sources of the same survey at 325 MHz with similar flux densities. Most objects have a spectral index of the unresolved flux densities < -0.7. Whereas the high-frequency flux densities from low-resolution surveys fit this slope, the flux densities at low frequencies, which were observed with a resolution $< 1'$, are significantly smaller because the object is resolved: the low-frequency emission is emitted only by a part of the object mimicking a flatter spectral index. Since the 325 MHz flux density has to fit the low- and high-frequency spectrum, these cases merely represent $< 20\,\%$.

In Fig. 10 three examples of PS source candidates are presented. In the top row of the figure, the resulting spectral fits of SPECFIND V3.0 are shown. In the bottom row, we show the results of the subsamples with the selection frequency (325 MHz or 1.4 GHz) marked by a dashed line. For the MPS source candidate NVSS J123048+485758 on the left (I), SPECFIND fitted mostly negative spectral slopes by excluding the three low-frequency spectral points. One positive slope was found by SPECFIND by ignoring several frequency points as well. The plot below shows that we were able to find the spectral break at around 360 MHz by dividing the frequency sample. For the concave source candidate NVSS J080637+774606 in the middle column (II), the peak spectral point at 1.4 GHz was ignored in the spectral fit of SPECFIND and thus the spectrum becomes flat. By using the two subsample catalogs, we were able to reveal the spectral break around 1.4 GHz. For the GPS source candidate NVSS J120215+720024 on the right (III), SPECFIND V3.0 did not include the low-frequency points and thus no spectral break is visible in the upper plot. Looking below, the plot includes all data points and thus a spectral break is identified at 1.4 GHz.

Doing this analysis on a sample with inhomogeneously obtained flux density measurements in the radio continuum, several caveats and biases need to be mentioned. Here, we discuss the important ones.

Flux density scales: Different radio surveys are known to have different flux density scales. We checked all catalog tables against the NVSS and SUMSS. Following Vollmer et al. (2005), the uncertainty in the flux density is measured as follows: $\Delta S = (S_{\rm extr} - S_{\rm cat})/S_{\rm cat}$, where $S_{\rm cat}$ is the flux density from NVSS or SUMSS. We applied a linear regression to all flux densities and the associated uncertainties of SPECFIND objects, which contain NVSS or SUMSS sources. $S_{\rm extr}$ is the flux density at 1.4 GHz of an object as calculated using the fitted SPECFIND spectrum. Spectral breaks are not taken into account. By fitting a Gaussian to the distribution of ΔS, we found that the relative offsets are in most cases comparable to the error of the measurements (Fig. A.2). The maximum ΔS of the processed cat-

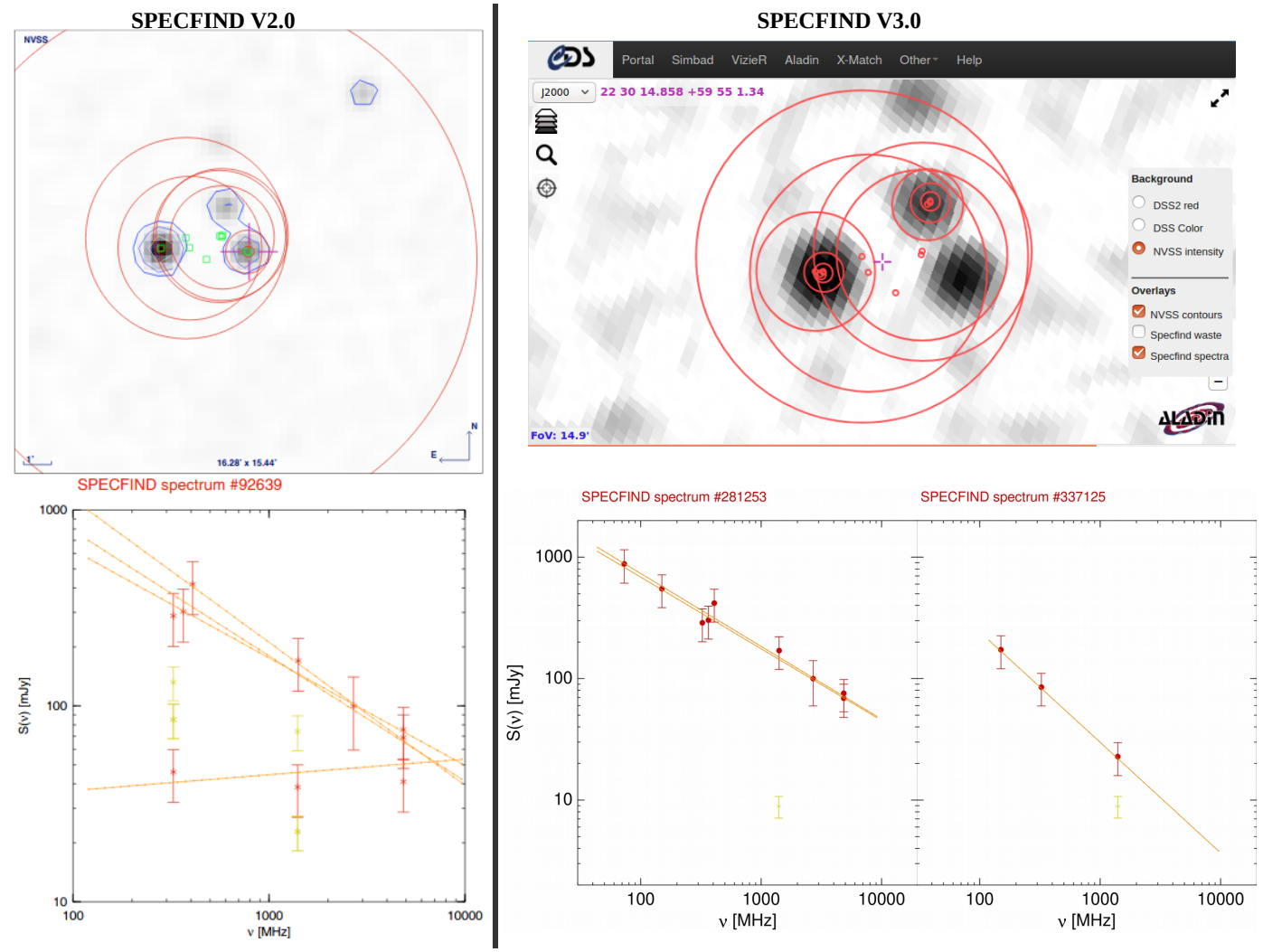

Fig. 7: Comparison of the resulting spectra around source WN B2228.5+5939 for SPECFIND V2.0 and V3.0. Top: NVSS grayscale and blue contours. Red circles are the beams of the catalogs included in the spectrum. Bottom: Spectra of the SPECFIND versions. While both versions are only able to reproduce two out of the three sources, SPECFIND V3.0 is able to separate these into two individual spectra.

alogs is 12 %. Only 6 small catalogs show ΔS larger than 10 % (ATESP, B3a, [RLM94], [JAP2011], [HFT2009]4, PiGSS-L). 94 out of 147 catalogs show ΔS smaller than 5 %. The statistical uncertainty or the standard deviation of the distribution increases the uncertainties of the spectral slopes, and the offsets lead to systematically lower or higher spectral indices (see Sect. 4.3). Such systematic uncertainties introduce biases in our source selections and decrease the completeness of our sample. The effect is expected (i) to decrease with an increasing number of independent flux densities within a spectrum and (ii) to be most important if the flux densities at the break frequency are affected by strong systematic uncertainties. In order to take the statistical and systematic uncertainties of the flux densities into account, the SPECFIND tool increases all flux density errors to 30 % for the cross-identification, effectively smoothing out these variations but still maintaining sufficient precision to carry out the analysis. This procedure smooths spectral structure and decreases the completeness of our sample.

Spatial scales: Different interferometers are sensitive to different spatial scales on the sky. Therefore, the flux density measurements and thus the spectra can be influenced by different Fourier sampling of the source. To quantify this effect, we compared the flux densities of sources with both NVSS and FIRST14 data. For 4800 sources in our spectral break sample, which have both flux density measurements, we find a median flux density difference of 2.8% between the two surveys. Furthermore, the SPECFIND tool selects flux measurements that are consistent with a single spectral slope. If a source is resolved for the minority of the flux density measurements, SPECFIND will discard these lower flux density measurements (see left panel of Fig. 8). However, in the rather unlikely case that a source were only resolved in the low-frequency regime, this could lead to a concave spectrum.

Observation dates - variable sources: PS sources are expected to be variable. To deal with a limited amount of source variability, the SPECFIND tool increases the flux error to 30% for the cross-identification. Since the vast majority of the frequency measurements used in SPECFIND are uncorrelated in time, SPECFIND is able to pick out the flux measurements that are consistent with a single spectral slope. However, the smaller the number of cross-identified flux density measurements, the

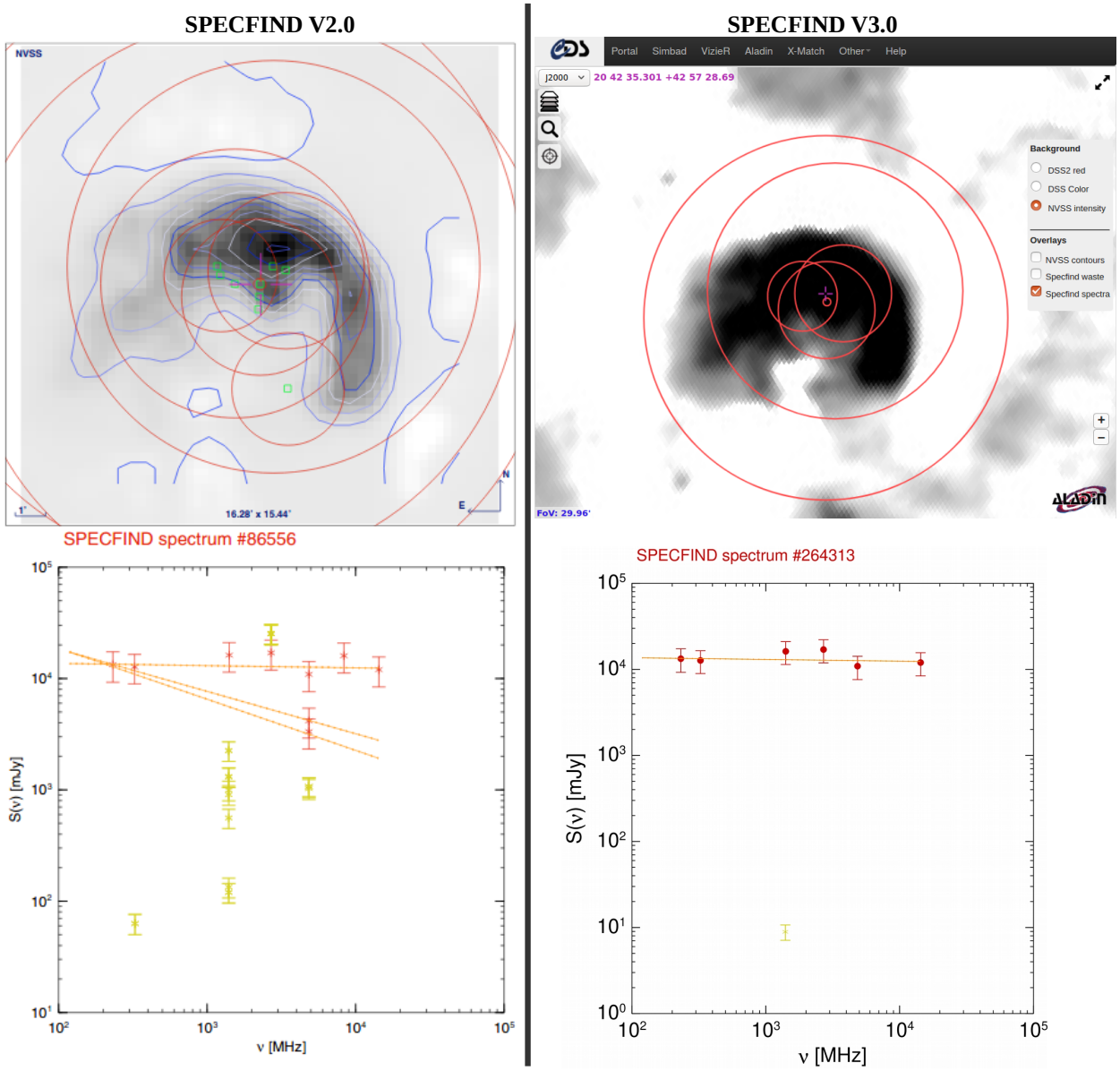

Fig. 8: Comparison of the resulting spectra of source WN B2040.8+4246 for SPECFIND V2.0 and V3.0. Top: NVSS grayscale and blue contours. Red circles are the beams of the catalogs included in the spectrum. Bottom: Spectra of the SPECFIND versions. In SPECFIND V3.0 one clear slope is visible.

higher the probability of a random cross-identification. Variability can occur on timescales of years at megahertz frequencies. At high frequencies ($\sim$ 10 GHz) the variability timescale can be much shorter. Since SPECFIND PS sources have at least two flux densities measured at frequencies above the break frequency and two flux densities measured at frequencies below the break frequency, the probability of a random cross-identification is rather limited, especially at high frequencies where timescales are short.

With a frequency cut at 1.4 GHz we found 2908 spectral break source candidates, 110 concave spectrum source candidates, and 86 GPS source candidates (15 examples shown in Table B.1). With a frequency cut at 325 MHz we found 17 201 spectral break source candidates, 327 concave source candidates, and 547 MPS source candidates (15 examples shown in Table B.2). About 70 % of our spectral break/PS sources are compact (see appendix section B.4). The full list of spectral break sources is available via the VizieR database. The description of the sample properties and their comparison with two recent samples of PS sources (Callingham et al. 2017; Sotnikova et al. 2019) are presented in Appendix B.

As expected, our GPS/MPS sample is far from being complete. The comparison with the results of Callingham et al. (2017) showed that we could only correctly identify $\sim$ 23 % of their PS sources. We were able to find about 50 % of their PS sources with a flux density in excess of 0.16 Jy at 200 MHz in our spectral break samples. This is caused by the fact that SPECFIND needs at least 5 flux density measurements at independent frequencies with inhomogeneous coverages and sensitivities of the input catalogs. We call this effect the catalog selection bias. For example, the GPS sources PKS 1934-638 and PKS 0008-421 are not present in the SPECFIND PS source candidate samples. PKS 1934-638 has a peak frequency at $\sim$ 1.4 GHz. Since there is no flux density measurement at

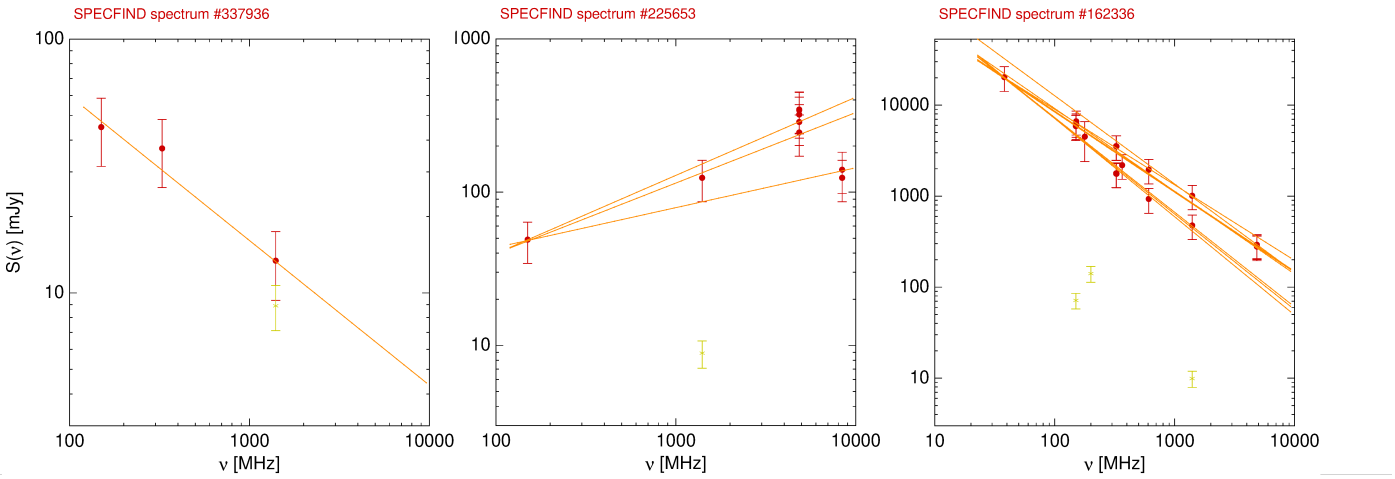

Fig. 9: Example spectra of new sources in SPECFIND V3.0. Left: NVSS J135722+732125 with three spectral points, including the ones from WSTBa and TGSSADR. Middle: NVSS J171701+191740 with ten spectral points and a possible turnover. Right: Double source NVSS J123317+670808 with twenty spectral points. The two slightly separated slopes indicate two sources.

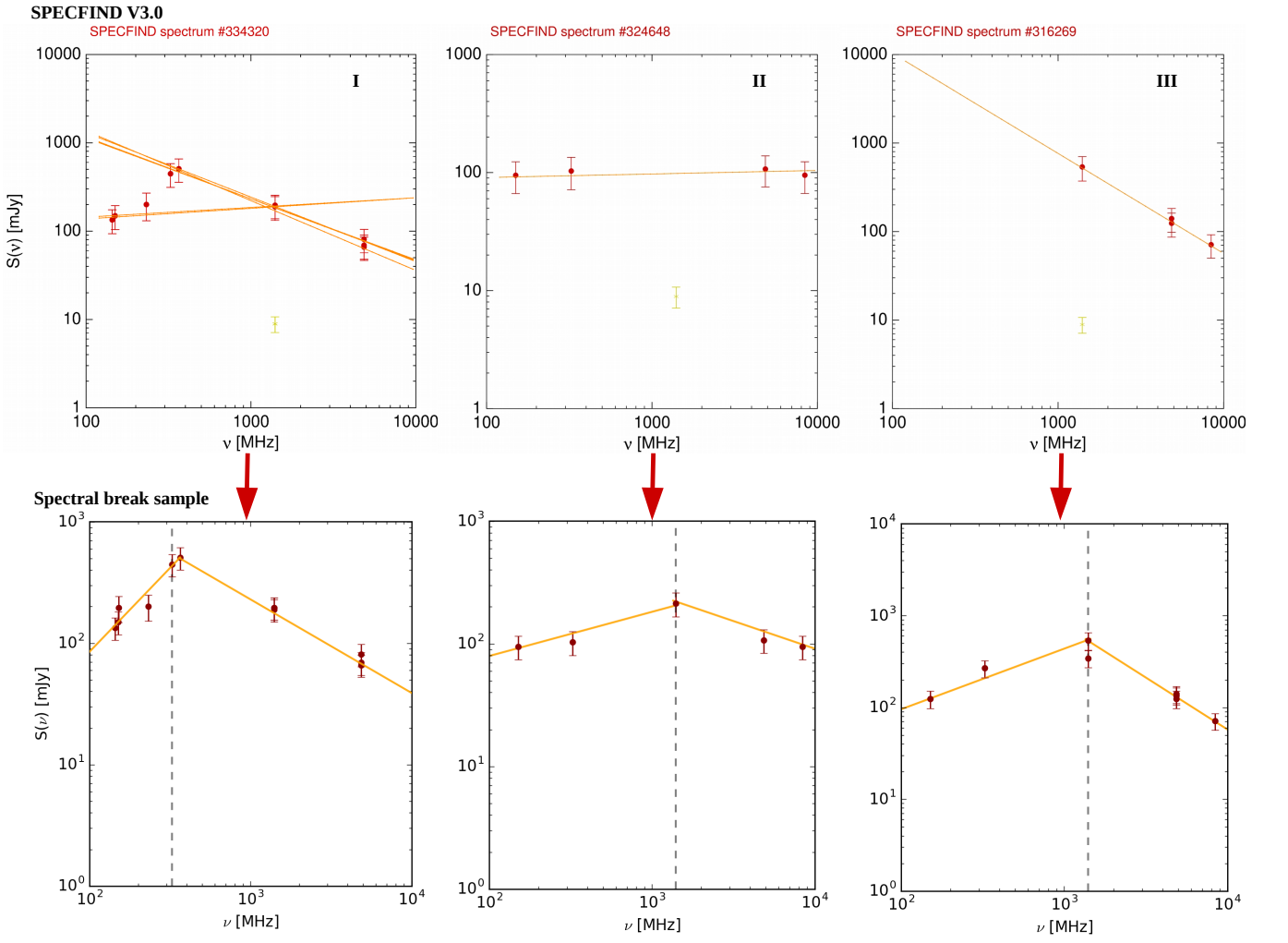

Fig. 10: Examples of three spectral break sources of our samples. Top row: Spectral fit of SPECFIND V3.0. Bottom row: Spectral fit of the spectral break with vertical dashed line at the selection frequency, where the subsamples were divided. Left: MPS source candidate NVSS J123048+485758. In SPECFIND V3.0 the left part of the spectrum was ignored for most of the spectral fits. Middle: Concave source candidate NVSS J080637+774606. The peak frequency point at 1.4 GHz was not included in SPECFIND V3.0. Right: GPS source candidate NVSS J120215+720024. The low-frequency part of the spectrum was not included in SPECFIND V3.0.

this frequency in SPECFIND V3.0, the object was missed. It would have been there with the AT20G catalog and will certainly be there with the Australien Square Kilometer Array Pathfinder (ASKAP) Evolutionary Map of the Universe (EMU) catalog. PKS 0008-421 has a peak frequency at ∼ 600 MHz and is present in the SPECFIND V3.0 catalog with the two spectral slopes. Since the two spectra could not meet in a common point around the peak frequency, this object is not present in the SPECFIND PS source candidate samples. It would have been there with the AT20G or PKS90 catalogs and will certainly be there with the ASKAP EMU catalog. On the other hand, the five 3C sources (3C 48, 3C 49, 3C 138, 3C 277, and 3C 287) presented in Murgia et al. (1999) are all identfied as spectral break (325 MHz) objects by SPECFIND. In addition, the nine GPS sources presented in Stanghellini et al. (1997) are all identified as HFP sources (in the main catalog) or spectral break sources (at 1.4 GHz) by SPECFIND and 36 out of the 49 Parkes half-Jansky GPS radio galaxies (Snellen et al. 2002) are identified as GPS/MPS sources by SPECFIND[7].

The fraction of false positives in our GPS/MPS source candidate samples is $\lesssim 20\,\%$. Up to about half of our MPS source candidates, which are not present in the Callingham et al. (2017) sample, or up to $\sim 25\,\%$ of our MPS source candidate sample probably are flat spectrum sources with strong variability at frequencies in excess of 1 GHz. Since our PS source candidate samples are not complete, we warrant caution using these samples for population studies of PS sources.

6. The VizieR SPECFIND V3.0 catalog

SPECFIND V3.0 is accessible via VizieR. By typing "specfind" in the main search field of VizieR, the SPECFIND V3.0 catalog will be visible. The general structure is the same as in SPECFIND V2.0, but with five instead of three tables within the main SPECFIND V3.0 catalog. These tables are named "spectra," "beam," "waste," "ghzbreak_cand" and "mhzbreak_cand."

The main result is presented in table "spectra" with every radio continuum source that have one entry row (see Fig. B.6 for the first rows of the VizieR table). The different objects/spectra are gathered by different sequence numbers (column "Seq"). All radio continuum sources with the same sequence number belong to the same object/spectrum. In the second column, the source name is given followed by the number of sources within the spectrum ("N"). The columns "a" and "b" are the spectral index and the abscissa of the spectral fit, respectively. The column "nu" contains the frequency of the catalog, followed by the flux density "S(nu)", its error "e" and the position of the source (Right Ascension and Declination). The column "SED" is a link to the spectral fit, which is the spectrum containing this source. The column "Radio+Opt" launches an Aladin Lite (Boch & Fernique 2014)[8] view of the source. The last column gives the beam size of the observation.

The "beam" table contains all 204 catalog tables from the 160 VizieR catalogs that were used in SPECFIND V3.0. It is similar to Table A.1. The "waste" table has the same general structure as "spectra," but contains measurements that were cross-identified by position but did not match the power-law spectrum. These points are included to the VizieR SED plot as well.

The spectral break sources are provided in two different tables. The table "ghzbreak_cand" contains all 3104 spectral break sources with turnover frequencies around 1.4 GHz including the 196 PS (concave/GPS) source candidates. The table "mhzbreak_cand" lists the 18 075 spectral break sources with turnover frequencies around 325 MHz including the 874 PS (concave/MPS/GMPS) sources. The structure of the tables is similar to the spectra table. The first column gives the running number "No." The sources belonging to the same spectrum have the same number. The second column provides the source name. The column "cat" gives the type (spectral break (sb), concave (conc), GPS/MPS (gps/mps)), followed by the column "resolved" including the information if the source is resolved (1) or not (0), the spectral slope and the abscissa associated with the source. In the next column, α_{low}, the mean spectral slope of the lower-frequency part is given, followed by its error. In the next column, α_{high}, the mean spectral slope of higher-frequency part is given, followed by its error. Then the frequency, the flux density and its error are listed. Lastly, the position (Right Ascension and Declination) and the beam/resolution are specified.

7. Summary and conclusions

We present a new version of SPECFIND, which has been successfully upgraded from 115 catalog tables in version 2.0 to version 3.0 with a final number of 204 processed catalog tables originating from 160 VizieR catalogs. 89 new catalog tables were ingested and two catalog tables were updated. The final number of resulting spectra was increased by more than a factor of three from ∼107 500 in version 2.0 to ∼340 000 in version 3.0. The number of objects with cross-identified sources was more than doubled from ∼600 000 in version 2.0 to ∼1.6 million in version 3.0. In comparison to the former version, more confused sources are separated into different objects. Nevertheless some spectra contain multiple sources and we note that the user should always check the spectra via the VizieR link to Aladin Lite within the catalog.

The 204 processed catalog tables span a wide frequency range between 16.7 MHz to 31 GHz, and cover major parts of the sky. The new low-frequency radio catalogs with large sky coverages represent important input data for SPECFIND V3.0. By applying SPECFIND on two subsamples of the catalogs with frequency cuts at 325 MHz and 1.4 GHz, 20 982 unique spectral break and 633 PS source candidates could be identified. A conservative estimate of the resolved PS sources fraction is about 30 %. The comparison with the results of Callingham et al. (2017) showed that we could find about half of their PS sources in our spectral break sample due to our selection bias. About 23 % of their PS sources could be consistently classified. The fraction of false positives in our PS candidate sample is estimated to be at maximum 20 %. We encourage follow-up observations of these candidates to confirm their nature.

SPECFIND is based on the radio catalogs in VizieR, and as described, the results of SPECFIND are integrated back into VizieR as a value-added compilation with accompanying services for visualization and access to the data. Moreover, the cross-identified radio continuum sources will be ingested into the SIMBAD astronomical database. This is part of the global effort to make astronomy data interoperable, with the objective of enabling new science with combined data sets. SPECFIND is an example of interoperability based on standardization of spectral properties, and using this to unify data extracted from hundreds of individually published and heterogeneous catalogs. IVOA and CDS standards play an important role for combining

[7] The other sources are present in the SPECFIND catalog but could not be identified as GPS/MPS sources mainly because of an insufficient number of flux density measurements.

[8] https://aladin.u-strasbg.fr/aladin.gml

data in SPECFIND, and we anticipate that interoperability of data over many spectral regimes and also for time domain data will open many new areas of research based on combined data.

Acknowledgements. This research has made use of the VizieR catalog access tool, CDS, Strasbourg, France (DOI: 10.26093/cds/vizier). The original description of the VizieR service was published in A&AS 143, 23 This research has made use of "Aladin sky atlas" developed at CDS, Strasbourg Observatory, France published in 2000A&AS..143...33B and 2014ASPC..485..277B. This research has made use of the SIMBAD database, operated at CDS, Strasbourg, France.

References

Ainsworth, R. E., Coughlan, C. P., Green, D. A., Scaife, A. M. M., & Ray, T. P. 2016, MNRAS, 462, 2904
Allen, M. G., Ochsenbein, F., Derriere, S., et al. 2014, in Astronomical Society of the Pacific Conference Series, Vol. 485, Astronomical Data Analysis Software and Systems XXIII, ed. N. Manset & P. Forshay, 219
Altenhoff, W. J., Downes, D., Pauls, T., & Schraml, J. 1979, A&AS, 35, 23
Altschuler, D. R. 1986, A&AS, 65, 267
AMI Consortium, Davies, M. L., Franzen, T. M. O., et al. 2011, MNRAS, 415, 2708
Angelakis, E., Kraus, A., Readhead, A. C. S., et al. 2009, A&A, 501, 801
Baldwin, J. E., Boysen, R. C., Hales, S. E. G., et al. 1985, MNRAS, 217, 717
Becker, R. H., White, R. L., & Edwards, A. L. 1991, ApJS, 75, 1
Becker, R. H., White, R. L., Helfand, D. J., & Zoonematkermani, S. 1994, ApJS, 91, 347
Benn, C. R. 1995, MNRAS, 272, 699
Benn, C. R., Grueff, G., Vigotti, M., & Wall, J. V. 1982, MNRAS, 200, 747
Benn, C. R. & Kenderdine, S. 1991, MNRAS, 251, 253
Bennett, A. S. 1962, MmRAS, 68, 163
Bennett, C. L., Lawrence, C. R., Burke, B. F., Hewitt, J. N., & Mahoney, J. 1986, ApJS, 61, 1
Biggs, A. D. & Ivison, R. J. 2006, MNRAS, 371, 963
Bihr, S., Johnston, K. G., Beuther, H., et al. 2016, A&A, 588, A97
Boch, T. & Fernique, P. 2014, in Astronomical Society of the Pacific Conference Series, Vol. 485, Astronomical Data Analysis Software and Systems XXIII, ed. N. Manset & P. Forshay, 277
Bondi, M., Ciliegi, P., Zamorani, G., et al. 2003, A&A, 403, 857
Bourda, G., Charlot, P., Porcas, R. W., & Garrington, S. T. 2010, A&A, 520, A113
Bower, G. C., Croft, S., Keating, G., et al. 2010, ApJ, 725, 1792
Braude, S. I., Megn, A. V., Rashkovskii, S. L., et al. 1978, Ap&SS, 54, 37
Callingham, J. R., Ekers, R. D., Gaensler, B. M., et al. 2017, ApJ, 836, 174
Carroll, P. A., Line, J., Morales, M. F., et al. 2016, MNRAS, 461, 4151
Charlot, P., Boboltz, D. A., Fey, A. L., et al. 2010, AJ, 139, 1713
Chiappetti, L., Pierre, M., Adami, C., et al. 2018, VizieR Online Data Catalog, IX/52
Ciliegi, P., McMahon, R. G., Miley, G., et al. 1999, MNRAS, 302, 222
Cohen, A. S., Lane, W. M., Cotton, W. D., et al. 2007, AJ, 134, 1245
Cohen, A. S., Röttgering, H. J. A., Jarvis, M. J., Kassim, N. E., & Lazio, T. J. W. 2004, ApJS, 150, 417
Coleman, P. H., Condon, J. J., & Hazard, C. 1985, AJ, 90, 1437
Condon, J. J. 1992, ARA&A, 30, 575
Condon, J. J., Anderson, E., & Broderick, J. J. 1995, AJ, 109, 2318
Condon, J. J., Cotton, W. D., Greisen, E. W., et al. 1998, AJ, 115, 1693
Coppejans, R., Cseh, D., Williams, W. L., van Velzen, S., & Falcke, H. 2015, MNRAS, 450, 1477
Croft, S., Bower, G. C., & Whysong, D. 2013, ApJ, 762, 93
De Breuck, C., Tang, Y., de Bruyn, A. G., Röttgering, H., & van Breugel, W. 2002, A&A, 394, 59
de Vries, W. H., Morganti, R., Röttgering, H. J. A., et al. 2002, AJ, 123, 1784
Derriere, S., Gray, N., McDowell, J. C., et al. 2004, in Astronomical Society of the Pacific Conference Series, Vol. 314, Astronomical Data Analysis Software and Systems (ADASS) XIII, ed. F. Ochsenbein, M. G. Allen, & D. Egret, 315
Douglas, J. N., Bash, F. N., Bozyan, F. A., Torrence, G. W., & Wolfe, C. 1996, AJ, 111, 1945
Dressel, L. L. & Condon, J. J. 1978, ApJS, 36, 53
Durdin, J. M., Pleticha, D., Condon, J. J., et al. 1975, National Astronomy and Ionospheric Center Report, 45, 1
Edge, D. O., Shakeshaft, J. R., McAdam, W. B., Baldwin, J. E., & Archer, S. 1959, MmRAS, 68, 37
Fanti, C., Fanti, R., Ficarra, A., & Padrielli, L. 1974, A&AS, 18, 147
Fanti, C., Mantovani, F., & Tomasi, P. 1981, A&AS, 43, 1
Fanti, C., Pozzi, F., Dallacasa, D., et al. 2001, A&A, 369, 380
Fanti, R., Fanti, C., Schilizzi, R. T., et al. 1990, A&A, 231, 333
Feain, I. J., Ekers, R. D., Murphy, T., et al. 2009, ApJ, 707, 114
Ficarra, A., Grueff, G., & Tomassetti, G. 1985, A&AS, 59, 255
Fich, M. 1986, AJ, 92, 787
Filipović, M. D., Bohlsen, T., Reid, W., et al. 2002, MNRAS, 335, 1085
Filipovic, M. D., Haynes, R. F., White, G. L., et al. 1995, A&AS, 111, 311
Forkert, T. & Altschuler, D. R. 1987, A&AS, 70, 77
Franzen, T. M. O., Banfield, J. K., Hales, C. A., et al. 2015, MNRAS, 453, 4020
Furst, E., Reich, W., Reich, P., & Reif, K. 1990, A&AS, 85, 805
Garn, T., Green, D. A., Hales, S. E. G., Riley, J. M., & Alexander, P. 2007, MNRAS, 376, 1251
Garn, T., Green, D. A., Riley, J. M., & Alexand er, P. 2008, MNRAS, 383, 75
Garn, T. S., Green, D. A., Riley, J. M., & Alexander, P. 2010, Bulletin of the Astronomical Society of India, 38, 103
Ghosh, A., Prasad, J., Bharadwaj, S., Ali, S. S., & Chengalur, J. N. 2012, MNRAS, 426, 3295
Gower, J. F. R., Scott, P. F., & Wills, D. 1967, MmRAS, 71, 49
Green, D. A. & Riley, J. M. 1995, MNRAS, 274, 324
Gregorini, L., de Ruiter, H. R., Parma, P., et al. 1994, A&AS, 106, 1
Gregorini, L., Vigotti, M., Mack, K. H., Zoennchen, J., & Klein, U. 1998, A&AS, 133, 129
Gregory, P. C. & Condon, J. J. 1991, ApJS, 75, 1011
Gregory, P. C., Scott, W. K., Douglas, K., & Condon, J. J. 1996, ApJS, 103, 427
Griffith, M., Langston, G., Heflin, M., Conner, S., & Burke, B. 1991, ApJS, 75, 801
Hales, S. E. G., Baldwin, J. E., & Warner, P. J. 1993, MNRAS, 263, 25
Hardcastle, M. J., Gürkan, G., van Weeren, R. J., et al. 2016, MNRAS, 462, 1910
Haynes, R. F., Caswell, J. L., & Simons, L. W. J. 1979, Australian Journal of Physics Astrophysical Supplement, 48, 1
Healey, S. E., Fuhrmann, L., Taylor, G. B., Romani, R. W., & Readhead, A. C. S. 2009, AJ, 138, 1032
Healey, S. E., Romani, R. W., Taylor, G. B., et al. 2007, ApJS, 171, 61
Helfand, D. J., White, R. L., & Becker, R. H. 2015, ApJ, 801, 26
Helmboldt, J. F., Taylor, G. B., Tremblay, S., et al. 2007, ApJ, 658, 203
Herrera Ruiz, N., Middelberg, E., Deller, A., et al. 2017, A&A, 607, A132
Heywood, I., Jarvis, M. J., Baker, A. J., et al. 2016, MNRAS, 460, 4433
Hodge, J. A., Becker, R. H., White, R. L., Richards, G. T., & Zeimann, G. R. 2011, AJ, 142, 3
Hopkins, A. M., Mobasher, B., Cram, L., & Rowan-Robinson, M. 1998, MNRAS, 296, 839
Hurley-Walker, N., Callingham, J. R., Hancock, P. J., et al. 2017a, MNRAS, 464, 1146
Hurley-Walker, N., Callingham, J. R., Hancock, P. J., et al. 2017b, MNRAS, 464, 1146
Huynh, M. T., Jackson, C. A., Norris, R. P., & Prand oni, I. 2005, AJ, 130, 1373
Ibar, E., Ivison, R. J., Biggs, A. D., et al. 2009, MNRAS, 397, 281
Intema, H. T., Jagannathan, P., Mooley, K. P., & Frail, D. A. 2017a, A&A, 598, A78
Intema, H. T., Jagannathan, P., Mooley, K. P., & Frail, D. A. 2017b, A&A, 598, A78
Intema, H. T., van Weeren, R. J., Röttgering, H. J. A., & Lal, D. V. 2011, A&A, 535, A38
Ishwara-Chandra, C. H., Sirothia, S. K., Wadadekar, Y., Pal, S., & Windhorst, R. 2010, MNRAS, 405, 436
Jackson, N., Roland, J., Bremer, M., Rhee, G., & Webb, J. 1999, A&AS, 134, 401
Jacobs, D. C., Aguirre, J. E., Parsons, A. R., et al. 2011, ApJ, 734, L34
Joncas, G. & Higgs, L. A. 1990, A&AS, 82, 113
Jones, P. A. & McAdam, W. B. 1992, ApJS, 80, 137
Kassim, N. E. 1988, ApJS, 68, 715
Kellermann, K. I., Fomalont, E. B., Mainieri, V., et al. 2008, ApJS, 179, 71
Kerton, C. R., Murphy, J., & Patterson, J. 2007, MNRAS, 379, 289
Kollgaard, R. I., Brinkmann, W., Chester, M. M., et al. 1994, ApJS, 93, 145
Kulkarni, V. K., Mantovani, F., & Pauliny-Toth, I. I. K. 1990, A&AS, 82, 41
Lane, W. M., Cotton, W. D., van Velzen, S., et al. 2014, MNRAS, 440, 327
Langston, G., Minter, A., D'Addario, L., et al. 2000, AJ, 119, 2801
Large, M. I., Cram, L. E., & Burgess, A. M. 1991, The Observatory, 111, 72
Laurent-Muehleisen, S. A., Kollgaard, R. I., Ryan, P. J., et al. 1997, A&AS, 122, 235
Lawrence, C. R., Bennett, C. L., Garcia-Barreto, J. A., Greenfield, P. E., & Burke, B. F. 1983, ApJS, 51, 67
Leahy, D. A. & Roger, R. S. 1996, A&AS, 115, 345
Ledlow, M. J. & Owen, F. N. 1995, AJ, 109, 853
Lee, J. A., Sohn, B. W., Jung, T., Byun, D.-Y., & Lee, J. W. 2017, ApJS, 228, 22
Martinez, A. P., Louys, M., Cecconi, B., et al. 2018, The UCD1+ controlled vocabulary Version 1.3 Version 1.3, IVOA Recommendation 27 May 2018
Mason, B. S., Weintraub, L., Sievers, J., et al. 2009, ApJ, 704, 1433
Mauch, T., Klöckner, H.-R., Rawlings, S., et al. 2013, MNRAS, 435, 650
Mauch, T., Murphy, T., Buttery, H. J., et al. 2003, MNRAS, 342, 1117
McConnell, D., Sadler, E. M., Murphy, T., & Ekers, R. D. 2012, MNRAS, 422, 1527

Meyers, B. W., Hurley-Walker, N., Hancock, P. J., et al. 2017, PASA, 34, e013
Middelberg, E., Norris, R. P., Cornwell, T. J., et al. 2008, AJ, 135, 1276
Mingaliev, M. G., Sotnikova, Y. V., Mufakharov, T. V., Erkenov, A. K., & Udovitskiy, R. Y. 2013, VizieR Online Data Catalog (other), 0330, J/other/AstBu/68
Morganti, R., Garrett, M. A., Chapman, S., et al. 2004, A&A, 424, 371
Morrison, G. E., Owen, F. N., Dickinson, M., Ivison, R. J., & Ibar, E. 2010, ApJS, 188, 178
Muchovej, S., Leitch, E., Carlstrom, J. E., et al. 2010, ApJ, 716, 521
Murgia, M., Fanti, C., Fanti, R., et al. 1999, A&A, 345, 769
Murphy, T., Mauch, T., Green, A., et al. 2007, MNRAS, 382, 382
Murphy, T., Sadler, E. M., Ekers, R. D., et al. 2010, MNRAS, 402, 2403
Myers, S. T., Jackson, N. J., Browne, I. W. A., et al. 2003, MNRAS, 341, 1
Niklas, S., Klein, U., Braine, J., & Wielebinski, R. 1995, A&AS, 114, 21
Norris, R. P., Afonso, J., Appleton, P. N., et al. 2006, AJ, 132, 2409
Ochsenbein, F., Bauer, P., & Marcout, J. 2000, A&AS, 143, 23
O'Dea, C. P. 1998, PASP, 110, 493
O'Dea, C. P. & Saikia, D. J. 2021, A&A Rev., 29, 3
Offringa, A. R., Trott, C. M., Hurley-Walker, N., et al. 2016, MNRAS, 458, 1057
Oort, M. J. A. 1987, A&AS, 71, 221
Oort, M. J. A., Steemers, W. J. G., & Windhorst, R. A. 1988, A&AS, 73, 103
Owen, F. N., Morrison, G. E., Klimek, M. D., & Greisen, E. W. 2009, AJ, 137, 4846
Owen, F. N., White, R. A., Hilldrup, K. C., & Hanisch, R. J. 1982, AJ, 87, 1083
Pacholczyk, A. G. & Swihart, T. L. 1970, ApJ, 161, 415
Paladini, R., Burigana, C., Davies, R. D., et al. 2003, A&A, 397, 213
Pearson, T. J. 1975, MNRAS, 171, 475
Pearson, T. J. & Kus, A. J. 1978, MNRAS, 182, 273
Peel, M. W., Gawroński, M. P., Battye, R. A., et al. 2011, MNRAS, 410, 2690
Perley, R. A. 1982, AJ, 87, 859
Prandoni, I., Gregorini, L., Parma, P., et al. 2000, A&AS, 146, 41
Press, W. H., Teukolsky, S. A., Vetterling, W. T., & Flannery, B. P. 2002, Numerical recipes in C++ : the art of scientific computing
Pushkarev, A. B. & Kovalev, Y. Y. 2012, A&A, 544, A34
Quiniento, Z. M. & Cersosimo, J. C. 1993, A&AS, 97, 435
Rees, N. 1990, MNRAS, 244, 233
Reich, P., Reich, W., & Furst, E. 1997, A&AS, 126, 413
Reich, W., Fuerst, E., Haslam, C. G. T., Steffen, P., & Reif, K. 1984, A&AS, 58, 197
Reich, W., Fürst, E., Reich, P., et al. 2000, A&A, 363, 141
Reich, W., Reich, P., & Fuerst, E. 1990, A&AS, 83, 539
Rengelink, R. B., Tang, Y., de Bruyn, A. G., et al. 1997, A&AS, 124, 259
Righetti, G., Giovannini, G., & Feretti, L. 1988, A&AS, 74, 315
Riseley, C. J., Scaife, A. M. M., Hales, C. A., et al. 2016, MNRAS, 462, 917
Roettgering, H. J. A., Lacy, M., Miley, G. K., Chambers, K. C., & Saunders, R. 1994, A&AS, 108, 79
Ross, K., Callingham, J. R., Hurley-Walker, N., et al. 2021, MNRAS, 501, 6139
Schinzel, F. K., Petrov, L., Taylor, G. B., & Edwards, P. G. 2017, ApJ, 838, 139
Shimwell, T. W., Tasse, C., Hardcastle, M. J., et al. 2019a, A&A, 622, A1
Shimwell, T. W., Tasse, C., Hardcastle, M. J., et al. 2019b, A&A, 622, A1
Simpson, C., Martínez-Sansigre, A., Rawlings, S., et al. 2006, MNRAS, 372, 741
Sirothia, S. K., Dennefeld, M., Saikia, D. J., et al. 2009a, MNRAS, 395, 269
Sirothia, S. K., Saikia, D. J., Ishwara-Chandra, C. H., & Kantharia, N. G. 2009b, MNRAS, 392, 1403
Slee, O. B. 1995, Australian Journal of Physics, 48, 143
Slee, O. B., Roy, A. L., & Andernach, H. 1996, Australian Journal of Physics, 49, 977
Snellen, I. A. G., Lehnert, M. D., Bremer, M. N., & Schilizzi, R. T. 2002, MNRAS, 337, 981
Snellen, I. A. G., Schilizzi, R. T., de Bruyn, A. G., et al. 1998, A&AS, 131, 435
Sotnikova, Y. V., Mufakharov, T. V., Majorova, E. K., et al. 2019, Astrophysical Bulletin, 74, 348
Stanghellini, C., O'Dea, C. P., Baum, S. A., et al. 1997, A&A, 325, 943
Tasse, C., Cohen, A. S., Röttgering, H. J. A., et al. 2006, A&A, 456, 791
Tasse, C., Röttgering, H. J. A., Best, P. N., et al. 2007, A&A, 471, 1105
Taylor, A. R., Goss, W. M., Coleman, P. H., van Leeuwen, J., & Wallace, B. J. 1996, ApJS, 107, 239
Taylor, J. H., Manchester, R. N., & Lyne, A. G. 1993, ApJS, 88, 529
Taylor, M. 2011, TOPCAT: Tool for OPerations on Catalogues And Tables
Thorat, K., Subrahmanyan, R., Saripalli, L., & Ekers, R. D. 2013, ApJ, 762, 16
Tingay, S. J., Hancock, P. J., Wayth, R. B., et al. 2016, AJ, 152, 82
Tinti, S., Dallacasa, D., de Zotti, G., Celotti, A., & Stanghellini, C. 2005, A&A, 432, 31
van Weeren, R. J., Williams, W. L., Tasse, C., et al. 2014, ApJ, 793, 82
Visser, A. E., Riley, J. M., Roettgering, H. J. A., & Waldram, E. M. 1995, A&AS, 110, 419
Vollmer, B., Davoust, E., Dubois, P., et al. 2005a, A&A, 431, 1177
Vollmer, B., Davoust, E., Dubois, P., et al. 2005b, A&A, 436, 757
Vollmer, B., Gassmann, B., Derrière, S., et al. 2010, A&A, 511, A53
Vollmer, B., Krichbaum, T. P., Angelakis, E., & Kovalev, Y. Y. 2008, A&A, 489, 49
Waldram, E. M., Pooley, G. G., Davies, M. L., Grainge, K. J. B., & Scott, P. F. 2010, MNRAS, 404, 1005
Waldram, E. M., Pooley, G. G., Grainge, K. J. B., et al. 2003, MNRAS, 342, 915
Waldram, E. M., Yates, J. A., Riley, J. M., & Warner, P. J. 1996, MNRAS, 282, 779
Walterbos, R. A. M., Brinks, E., & Shane, W. W. 1985, A&AS, 61, 451
White, G. J., Pearson, C., Braun, R., et al. 2010, A&A, 517, A54
White, R. L. & Becker, R. H. 1992, ApJS, 79, 331
White, R. L., Becker, R. H., & Helfand, D. J. 2005, AJ, 130, 586
White, R. L., Becker, R. H., Helfand, D. J., & Gregg, M. D. 1997, ApJ, 475, 479
Whittam, I. H., Green, D. A., Jarvis, M. J., & Riley, J. M. 2017, MNRAS, 464, 3357
Whittam, I. H., Riley, J. M., Green, D. A., et al. 2016, MNRAS, 457, 1496
Wieringa, M. H. 1993, Bulletin d'Information du Centre de Donnees Stellaires, 43, 17
Wilkinson, P. N., Browne, I. W. A., Patnaik, A. R., Wrobel, J. M., & Sorathia, B. 1998, MNRAS, 300, 790
Williams, C. L., Hewitt, J. N., Levine, A. M., et al. 2012, ApJ, 755, 47
Williams, W. L., Intema, H. T., & Röttgering, H. J. A. 2013, A&A, 549, A55
Williams, W. L., van Weeren, R. J., Röttgering, H. J. A., et al. 2016, MNRAS, 460, 2385
Windhorst, R. A., van Heerde, G. M., & Katgert, P. 1984, A&AS, 58, 1
Wright, A. & Otrupcek, R. 1990, PKS Catalog (1990, 0
Wright, A. E., Griffith, M. R., Hunt, A. J., et al. 1996, ApJS, 103, 145
Wright, A. E., Wark, R. M., Troup, E., et al. 1991, MNRAS, 251, 330
Zhang, X., Zheng, Y., Chen, H., et al. 1997, A&AS, 121, 59
Zinn, P. C., Middelberg, E., Norris, R. P., et al. 2012, A&A, 544, A38
Zoonematkermani, S., Helfand, D. J., Becker, R. H., White, R. L., & Perley, R. A. 1990, ApJS, 74, 181

Appendix A: Additional tables and figures

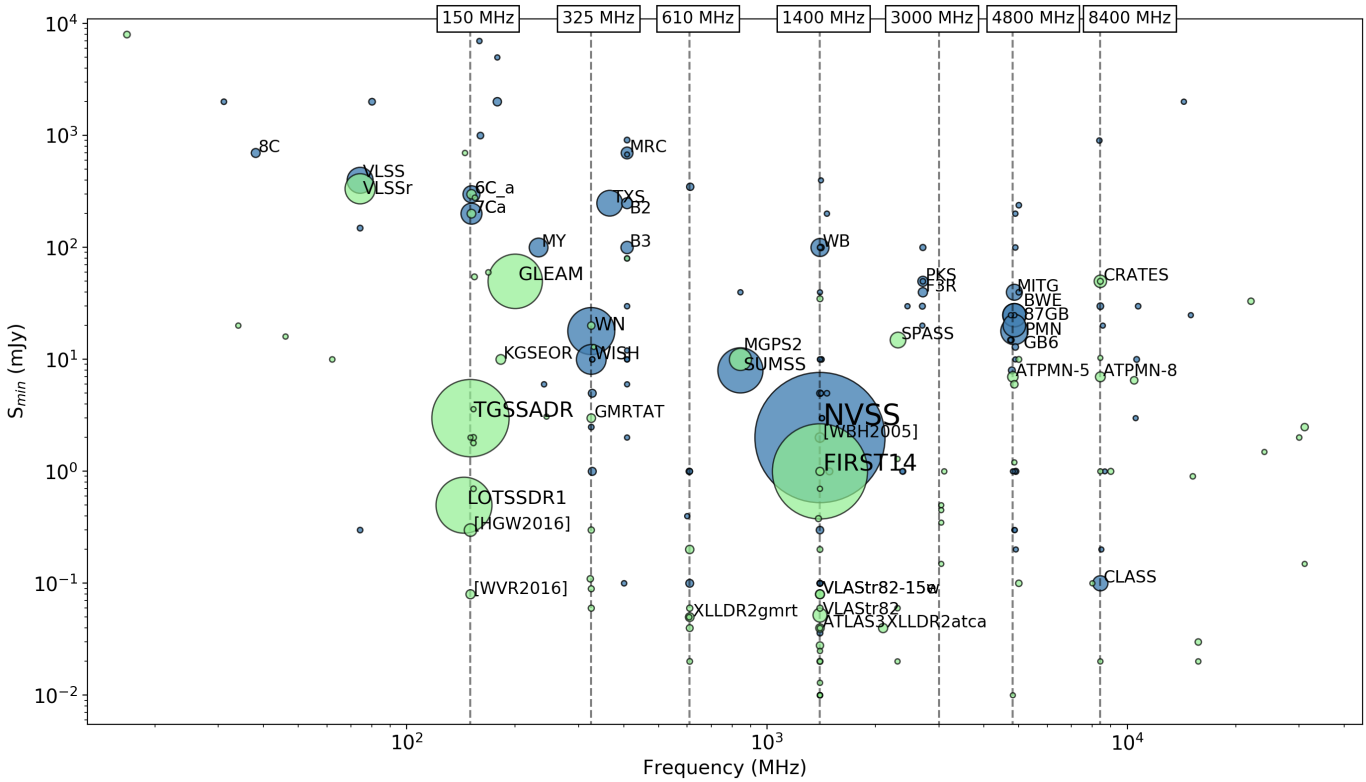

Fig. A.1: Minimum flux density (S_{min}) vs. frequency of the 204 catalog tables used in SPECFIND V3.0. The size of the circles represent the flux density measurement entries. Labeled catalogs have more than 5000 sources. Green shaded catalogs were added in version 3.0, blue shaded catalogs were already included in version 2.0.

Table A.1: Ingested catalogs of SPECFIND V3.0. This table is similar to table "beam.dat" in SPECFIND V3.0.

Name	Abrev	I	nu (MHz)	beam (arcmin)	Smin (mJy)	records	sp (%)	BibCode	VizieR Cat
[h!] NVSS	NVSS	I	1400	0.75	2	1773484	17.1	Condon et al. (1998)	VIII/65
FIRST14	FIRST14	I	1400	0.08333	1	946432	6.4	Helfand et al. (2015)	VIII/92
TGSSADR	TGSSADR	I	150	0.417	3	623604	46.5	Intema et al. (2017b)	J/A+A/598/A78
LOTSSDR1	ILT	I	144	0.417	0.5	325694	1.5	Shimwell et al. (2019b)	J/A+A/622/A1
GLEAM	GLEAM	I	200	2	50	307455	54.3	Hurley-Walker et al. (2017b)	VIII/100
WENSS	WN	I	325	0.2	18	229420	55.4	Rengelink et al. (1997)	VIII/62
SUMSS	SUMSS	I	843	0.3	8	211063	28.1	Mauch et al. (2003)	VIII/70
VLSSr	VLSSr	I	74	1.25	335	92965	72.1	Lane et al. (2014)	VIII/97
WISH	WISH	I	325	0.3	10	90357	60.2	De Breuck et al. (2002)	VIII/69
GB6	GB6	S	4850	1.8	18	75162	79.5	Gregory et al. (1996)	VIII/40
TXS	TXS	I	365	0.1	250	66841	72.2	Douglas et al. (1996)	VIII/42
87GB	87GB	S	4850	2.3	25	54579	82.6	Gregory & Condon (1991)	VIII/14
BWE	BWE	S	4850	2.3	25	53522	79.6	Becker et al. (1991)	VIII/13
PMN	PMN	S	4850	2.8	20	50814	57.9	Wright et al. (1996)	VIII/38
MGPS2	MGPS2	I	843	0.75	10	48850	16.2	Murphy et al. (2007)	VIII/82
7C	7C	I	151	1.17	200	43683	82.6	Visser et al. (1995)	VIII/84
MY	MY	I	232	2.5	100	34426	46.7	Zhang et al. (1997)	VIII/44
WB	WB	S	1400	2	100	31524	70.4	White & Becker (1992)	VIII/17
6C	6C	I	151	4.2	300	27666	87.2	Baldwin et al. (1985)	VIII/18,VIII/21-24
MITG	MITG	S	4850	4.3	40	24180	66.1	Bennett et al. (1986) - Griffith et al. (1991)	VIII/52
SPASS	SPASS	S	2307	10.75	15	23389	65	Meyers et al. (2017)	J/other/PASA/34.13
CLASS	CLASS	I	8400	0.0055	0.1	21486	43.5	Myers et al. (2003)	VIII/72
VLAStr82	[HBW2011]	I	1400	0.03	0.052	17969	2.2	Hodge et al. (2011)	J/AJ/142/3
[HGW2016]	[HGV2016]	I	150	0.13	0.3	13943	5.9	Hardcastle et al. (2016)	J/MNRAS/462/1910

Name	Abrev	I	nu (MHz)	beam (arcmin)	Smin (mJy)	records	sp (%)	BibCode	VizieR Cat
CRATES	CRATES	I	8400	0.1	50	13704	73.1	Healey et al. (2007)	J/ApJS/171/61
B3	B3	I	408	1.4	100	13340	77.4	Ficarra et al. (1985)	VIII/37
MRC	MRC	I	408	2	700	12141	92.2	Large et al. (1991)	VIII/16
B2	B2	I	408	5.2	250	9929	82.8	Fanti et al. (1974)	VIII/36
B2.1	B2.1	I	408	5.2	250	9929	82.8	1974AAS...18..147F	VIII/36
B2.2	B2.2	I	408	5.2	250	9929	82.8	1974AAS...18..147F	VIII/36
B2.3	B2.3	I	408	5.2	250	9929	82.8	1974AAS...18..147F	VIII/36
B2.4	B2.4	I	408	5.2	250	9929	82.8	1974AAS...18..147F	VIII/36
ATPMN-5	ATPMN5	IS	4800	0.03	7	9037	54.3	McConnell et al. (2012)	J/MNRAS/422/1527
PKS	PKS	S	2700	1	50	8264	81.4	Wright & Otrupcek (1990)	VIII/15
ATPMN-8	ATPMN8	IS	8400	0.02	7	7611	59.8	McConnell et al. (2012)	J/MNRAS/422/1527
KGSEOR	KGS	I	182	0.04	10	7394	68.4	Carroll et al. (2016)	J/MNRAS/461/4151
[WBH2005]	[WBH2005]	I	1400	0.1	2	6919	10.9	White et al. (2005)	J/AJ/130/586
6C_a	6Ca	I	151	4.2	300	6752	87.5	Hales et al. (1993)	VIII/25
F3R	F3R	S	2700	2.5	40	6495	73.2	Furst et al. (1990)	J/A+AS/85/805
XLLDR2atca	2XXL-ATCA	I	2100	0.08	0.04	6350	4.1	Chiappetti et al. (2018)	IX/52
[WVR2016]	[WVR2016]	I	150	0.1	0.08	6219	15.2	Williams et al. (2016)	J/MNRAS/460/2385
VLAStr82-15w	[HJB2016]w	I	1400	0.2	0.08	6094	3.4	Heywood et al. (2016)	J/MNRAS/460/4433
8C	8C	I	38	4.5	700	5859	72.6	Rees (1990)	VIII/31
VLAStr82-15e	[HJB2016]e	I	1400	0.2	0.08	5674	1.9	Heywood et al. (2016)	J/MNRAS/460/4433
7Ca	7Ca	I	151	1.17	200	5526	77.6	Waldram et al. (1996)	J/MNRAS/282/779
XLLDR2gmrt	XXL-GMRT	I	610	0.1	0.05	5434	11	Chiappetti et al. (2018)	IX/52
GMRTAT	[MKR2013]	S	325	0.3	3	5263	33.9	Mauch et al. (2013)	J/MNRAS/435/650
ATLAS3	ATLAS3	I	1400	0.17	0.04	5118	1.6	Franzen et al. (2015)	J/MNRAS/453/4020
GMRTLH2	GMRTLH	S	610	0.09	0.2	4934	7.3	Garn et al. (2010)	J/other/BASI/38.103
4C	4C	I	178	11.5	2000	4844	66.4	Gower et al. (1967)	VIII/4
[BJB2016]	[BJB2016]	I	1400	0.3	1	4422	3.8	Bihr et al. (2016)	J/A+A/588/A97
WSTBa	WSTBa	I	327	1	1	4157	48	Wieringa (1993)	VIII/19
WSRTGP	WSRTGP	I	327	1	5	3984	41.7	Taylor et al. (1996)	J/ApJS/107/239
FLSGMRT	FLSGMRT	I	610	0.1	0.1	3944	1.6	Garn et al. (2007)	J/MNRAS/376/1251
[AKR2009]4	[AKR2009]4	S	4850	2.4	6	3434	21.8	Angelakis et al. (2009)	J/A+A/501/801
[AKR2009]10	[AKR2009]10	S	10450	1.1	6.5	3434	22.1	Angelakis et al. (2009)	J/A+A/501/801
ATESP	ATESP	I	1400	0.23	0.3	3370	12.4	Prandoni et al. (2000)	VIII/63
SCG325	SCG325	I	325	0.217	20	3257	2.7	Riseley et al. (2016)	J/MNRAS/462/917
[DMR2002]	[DMR2002]	I	1400	0.31	0.028	3171	22.1	de Vries et al. (2002)	J/AJ/123/1784
LFRS31	[MWS2009]	I	31000	1.36	2.5	3164	21.9	Mason et al. (2009)	J/ApJ/704/1433
NAIC	NAIC	S	611	12.6	350	3122	50.4	Durdin et al. (1975)	VIII/61
GMRTEN1	GMRTEN1	I	610	0.1	0.04	2500	8.8	Garn et al. (2008)	J/MNRAS/383/75
NAICGB	NAICGB	S	4775	2.8	8	2453	74.9	Lawrence et al. (1983)	J/ApJS/51/67
VLA-NEP	VLA-NEP	I	1490	0.333	1	2435	17.9	Kollgaard et al. (1994)	J/ApJS/93/145
Cula	Cula	I	80	3.7	2000	2173	68.4	Slee (1995)	VIII/35
UTR-2	GRA	S	16.7	0.01	1.4	2129	2.2	Braude et al. (1978)	VIII/80
JVAS	JVAS	I	8400	0.0055	30	2121	85.1	Wilkinson et al. (1998)	VIII/60
Culb	Culb	I	160	1.85	1000	2042	82	Slee (1995)	VIII/35
GPSR	GPSR	I	1400	0.0833	5	1992	24.6	Zoonematkermani et al. (1990)	J/ApJS/74/181
R3FGL5	RFC5	I	5000	0.4	0.1	1894	25.7	Schinzel et al. (2017)	J/ApJ/838/139
10C-15	10C	I	15700	0.5	0.03	1888	21.9	AMI Consortium et al. (2011)	J/MNRAS/415/2708
RGB	RGB	I	4885	0.067	13	1861	76.1	Laurent-Muehleisen et al. (1997)	J/A+AS/122/235
RRF	RRF	S	1410	9.4	100	1830	77.2	Reich et al. (1997)	J/A+AS/83/539
KVNCS22	K-RFC	S	22000	2.1	33	1820	67.1	Lee et al. (2017)	J/ApJS/228/22
[ACG2016]323	[ACG2016]323	I	323	0.17	0.11	1815	10.1	Ainsworth et al. (2016)	J/MNRAS/462/2904
[CCW2015]	[CCW2015]	I	325	0.09	0.3	1706	52.3	Coppejans et al. (2015)	J/MNRAS/450/1477
WSTBb	WSTBb	I	608	0.5	1	1693	66.8	Wieringa (1993)	VIII/19
[IIB2009]a	[IIB2009]LH610MHz	I	610	0.08333	0.06	1619	2.8	Ibar et al. (2009)	J/MNRAS/397/281
[IIB2009]b	[IIB2009]LH1.4GHz	I	1400	0.08333	0.06	1479	3.3	Ibar et al. (2009)	J/MNRAS/397/281
[OMK2009]	[OMK2009]	I	324.5	0.1	0.06	1436	10.7	Owen et al. (2009)	J/AJ/137/4846
[PBD2003]	[PBD2003]	S	2700	8	100	1432	11.9	Paladini et al. (2003)	J/A+A/397/213
ATLBS	ATLBS	I	1388	0.83	0.38	1366	5.7	Thorat et al. (2013)	J/ApJ/762/16
R3FGL9	RFC9	I	9000	0.4	1	1351	32.5	Schinzel et al. (2017)	J/ApJ/838/139
[WIR2013]	[WIR2013]	I	153	0.42	2	1289	55.4	Williams et al. (2013)	J/A+A/549/A55
GPSR5	GPSR5	I	4900	0.067	1	1286	7.5	Becker et al. (1994)	J/ApJS/91/347
[SDS2009]	[SDS2009]GMRT	I	325	0.13	0.09	1285	11.6	Sirothia et al. (2009a)	J/MNRAS/395/269

Name	Abrev	I	nu (MHz)	beam (arcmin)	Smin (mJy)	records	sp (%)	BibCode	VizieR Cat
ATELAIS	ATELAIS	I	1400	0.5	35	1276	5	Middelberg et al. (2008)	J/AJ/135/1276
[MOD2010]	[MOD2010]	I	1400	0.05	0.02	1230	0.4	Morrison et al. (2010)	J/ApJS/188/178
RFS	RFS	S	2695	4.9	30	1212	34.8	Reich et al. (1984)	J/A+AS/58/197
PKS8400	PKS8400	S	8400	2.7	50	1192	76.2	Wright et al. (1991)	J/MNRAS/251/330
VIPS	VIPS	I	5000	0.000015	10	1119	67.6	Helmboldt et al. (2007)	J/ApJ/658/203
VIRMOS1400	VIRMOS1.4GHZ	I	1400	0.1	0.1	1103	3.5	Bondi et al. (2003)	J/A+A/403/857
[THW2016]154	[THW2016]MWA154	I	154	4	55	1085	74	Tingay et al. (2016)	J/AJ/152/82
PDF	PDF	I	1400	0.15	0.1	1079	3.2	Hopkins et al. (1998)	J/MNRAS/296/839
[MGC2004]	[MGC2004]	I	1400	0.23	0.036	1048	1.1	Morganti et al. (2004)	J/A+A/424/371
[TRB2007]b	[TRB2007]b	I	610	0.11	1	1037	33	Tasse et al. (2007)	J/A+A/471/1105
[FEM2009]	[FEM2009]	I	1400	0.76	0.2	1005	31.1	Feain et al. (2009)	J/ApJ/707/114
B3VLA	B3VLA	S	10600	1.15	10	981	80.2	Gregorini et al. (1998)	J/A+AS/133/129
ELAISR	ELAISR	I	1400	0.25	0.1	965	20.3	Ciliegi et al. (1999)	J/MNRAS/302/222
[CRJ2004]	[CRJ2004]	I	74	0.42	150	949	75.9	Cohen et al. (2004)	J/ApJS/150/417
DRAOP	DRAOP	I	408	3.5	915	915	67.3	Joncas & Higgs (1990)	VizieR VIII/55[(1)]
GMRTAMI	[WGJ2017]	I	610	0.12	0.02	913	3.6	Whittam et al. (2017)	J/MNRAS/464/3357
RRF	RRF	S	1410	9.4	100	884	40.1	Reich et al. (1990)	J/A+AS/83/539
[A86]	[A86]	S	4760	2.8	15	882	80.3	Altschuler (1986)	J/A+AS/65/267
UGC	UGC	S	2380	2.7	1	858	27.7	Dressel & Condon (1978)	J/ApJS/36/53
[TRC2006]a	[TRC2006]a	I	325	0.12	2.5	843	52	Tasse et al. (2006)	J/A+A/456/791
[NAA2006]	[NAA2006]	I	1400	0.12	0.04	784	5.7	Norris et al. (2006)	J/AJ/132/2409
[ISW2010]	[ISW2010]GMRT	I	153	0.27	0.7	765	43.9	Ishwara-Chandra et al. (2010)	J/MNRAS/405/436
B3a	B3a	S	4730	2.8	15	752	95.1	Kulkarni et al. (1990)	J/A+AS/82/41
RGB6	RGB6	S	5000	2.4	40	729	92.3	Reich et al. (2000)	J/A+A/363/141
[TRC2006]b	[TRC2006]b	I	74	0.5	0.3	725	0.1	Tasse et al. (2006)	J/A+A/456/791
[RLM94]	[RLM94]	I	1465	0.075	5	725	47.9	Roettgering et al. (1994)	J/A+AS/108/79
NEK	NEK	I	31	12	2000	703	4.6	Kassim (1988)	J/ApJS/68/715
NEK	NEK	I	30	12	2000	703	4.6	Kassim (1988)	J/ApJS/68/715
[HCS79]	[HCS79]	-	5000	0.54	240	702	7.8	Haynes et al. (1979)	VIII/20
RGB2	RGB2	S	10700	1.2	30	698	82.3	Reich et al. (2000)	J/A+A/363/141
[FBR2002]a	[FBR2002]a	I	2370	0.667	1	697	33.2	Filipović et al. (2002)	J/MNRAS/335/1085
RGB11	RGB11	S	2700	4.3	50	697	90.7	Reich et al. (2000)	J/A+A/363/141
[ACG2016]608	[ACG2016]608	I	608	0.17	0.05	687	7.4	Ainsworth et al. (2016)	J/MNRAS/462/2904
5C12a	5C12a	-	408	1.333	10	680	63.4	Benn & Kenderdine (1991)	VIII/30
[VWT2014]62	[VWT2014]62	I	62	0.4	10	658	64.8	van Weeren et al. (2014)	J/ApJ/793/82
[WHL2012b]	[WHL2012b]	I	154.24	15	280	648	68.6	Williams et al. (2012)	J/ApJ/755/47
9Ccont	9C	I	15200	0.4	0.9	643	50.6	Waldram et al. (2010)	J/MNRAS/404/1005
[ZSZ2012]	[ZSZ2012]	I	2300	0.5	0.06	631	10.1	Zinn et al. (2012)	J/A+A/544/A38
CRATES30	[PGB2011]	I	30000	1.2	2	605	59.6	Peel et al. (2011)	J/MNRAS/410/2690
[IWR2011]	[IVR2011]	I	153	0.4	1.8	597	79.9	Intema et al. (2011)	J/A+A/535/A38
MWAEOR	MWAEOR	I	168	2	60	586	90.1	Offringa et al. (2016)	J/MNRAS/458/1057
[ADP79]	[ADP79]	S	4875	2.6	100	569	25.1	Altenhoff et al. (1979)	J/A+AS/35/23
PSRa	PSRa	-	400	1	0.1	561	0.4	Taylor et al. (1993)	VII/189
GPA1	GPA1	S	8350	9.7	900	555	11.7	Langston et al. (2000)	J/AJ/119/2801
[BI2006]b	[BI2006]b	I	1400	0.024	0.01	537	0.7	Biggs & Ivison (2006)	J/MNRAS/371/963
WSTB	WSTB	I	1412	0.385	10	536	14.9	Windhorst et al. (1984)	J/A+AS/74/315
[FBR2002]	[FBR2002]	I	1420	1.633	3	534	45.1	Filipović et al. (2002)	J/MNRAS/335/1085
[SMR2006]	[SMR2006]VLA	I	1400	0.07	0.02	512	3.5	Simpson et al. (2006)	J/MNRAS/372/741
[BI2006]c	[BI2006]c	I	1400	0.025	0.01	506	4.1	Biggs & Ivison (2006)	J/MNRAS/371/963
32P	32P	I	408	4	30	494	65.5	Leahy & Roger (1996)	J/A+AS/115/345
10Ccont-15	10Ccont	I	15700	0.5	0.02	490	26.7	Whittam et al. (2016)	J/MNRAS/457/1496
[HMD2017]	[HMD2017]	I	1400	0.000014	0.013	488	0	Herrera Ruiz et al. (2017)	J/A+A/607/A132
ACOa	ACOa	S	1400	10	100	487	76.2	Owen et al. (1982)	VIII/29A
[JAP2011]	[JAP2011]	I	145	26	700	480	40.1	Jacobs et al. (2011)	J/ApJ/734/L34
3C	3C	I	159	10	7000	470	13.6	Edge et al. (1959)	VIII/1
[TRB2007]a	[TRB2007]a	I	240	0.25	6	466	67.2	Tasse et al. (2007)	J/A+A/471/1105
ATHDFS	ATHDFS	I	1400	0.11	0.01	466	1.1	Huynh et al. (2005)	J/AJ/130/1373
[WPB2010]	[WPB2010]NEP	I	1400	0.27	0.025	462	8.2	White et al. (2010)	J/A+A/517/A54
PSRc	PSRc	-	1400	1	0.1	445	0.5	Taylor et al. (1993)	VII/189
PiGSS	PiGSS	I	3100	1.6	1	423	73.2	Bower et al. (2010)	J/ApJ/725/1792
WSTB	WSTB	I	327	1.5	10	407	62	Oort et al. (1988)	J/A+AS/74/315
[P82a]	[P82a]	I	4885	0.1	200	404	75.1	Perley (1982)	J/AJ/87/859

Name	Abrev	I	nu (MHz)	beam (arcmin)	Smin (mJy)	records	sp (%)	BibCode	VizieR Cat
[P82]	[P82]	I	1465	0.43	200	404	84.7	Perley (1982)	J/AJ/87/859
IERS-S	IERS-S	I	2300	0.0002	1.3	398	30.3	Bourda et al. (2010)	J/A+A/520/A113
IERS-X	IERS-X	I	8400	0.00007	1	398	43.6	Bourda et al. (2010)	J/A+A/520/A113
[VWT2014]34	[VWT2014]34	I	34	0.68	20	392	52.2	van Weeren et al. (2014)	J/ApJ/793/82
MOST	MOST	I	843	0.733	40	384	73.5	Jones & McAdam (1992)	J/ApJS/80/137
51P	51P	I	408	4	80	383	72.9	Green & Riley (1995)	J/MNRAS/274/324
52P	52P	I	408	4	80	383	72.9	Green & Riley (1995)	J/MNRAS/274/324
ACO	ACO	I	1400	0.25	10	375	47.1	Ledlow & Owen (1995)	J/AJ/109/853
[PK2012]2	[PK2012]2IVS	I	2300	0.0004	0.02	370	53.6	Pushkarev & Kovalev (2012)	J/A+A/544/A34
[PK2012]8	[PK2012]8IVS	I	8400	0.000033	0.02	370	70.9	Pushkarev & Kovalev (2012)	J/A+A/544/A34
[FHW95]c	[FHW95]c	S	4750	4.8	15	368	53.9	Filipovic et al. (1995)	J/A+AS/111/311
[HFT2009]4	[HFT2009]4	I	4850	2.4	1.2	368	75.9	Healey et al. (2009)	J/AJ/138/1032
[VWT2014]46	[VWT2014]46	I	46	0.52	16	367	56.8	van Weeren et al. (2014)	J/ApJ/793/82
GPA	GPA	S	14350	6.6	2000	365	9.3	Langston et al. (2000)	J/AJ/119/2801
WSTB	WSTB	I	1412	0.385	10	359	8.1	Oort (1987)	J/A+AS/74/315
PSRb	PSRb	-	600	1	0.4	352	0.6	Taylor et al. (1993)	VII/189
IRAS	IRAS	S	4850	3.5	25	351	83.8	Condon et al. (1995)	J/AJ/109/2318
[FHW95]b	[FHW95]b	S	2450	8.85	30	334	54.9	Filipovic et al. (1995)	J/A+AS/111/311
3CR	3CR	I	178	6	5000	327	58.8	Bennett (1962)	VIII/1
[KFM2008]14	[KFM2008]14	I	1400	0.058	0.01	319	2.8	Kellermann et al. (2008)	J/ApJS/179/71
[SSI2009]153	[SSI2009]153	I	153	0.33	3.6	317	51.9	Sirothia et al. (2009b)	J/MNRAS/392/1403
[SSI2009]244	[SSI2009]244	I	244	0.2	3.1	317	56.9	Sirothia et al. (2009b)	J/MNRAS/392/1403
WSTB	WSTB	I	327	1.5	10	309	69	Righetti et al. (1988)	J/A+AS/74/315
5C12	5C12	I	408	1.5	2	308	81.9	Benn et al. (1982)	J/MNRAS/200/747
[SSI2009]1400	[SSI2009]1400	I	1400	0.04	0.7	303	62.8	Sirothia et al. (2009b)	J/MNRAS/392/1403
[JRB99]	[JRB99]	I	4860	0.03	1	298	23.8	Jackson et al. (1999)	J/A+AS/134/401
R3FGL8	RFC8	I	8000	0.4	0.1	290	76.6	Schinzel et al. (2017)	J/ApJ/838/139
5C6	5C6	I	408	1.5	6	267	75.8	Pearson & Kus (1978)	J/MNRAS/182/273
[CBF2010]24	[LBC2010]	I	24000	0.008	1.5	265	18.4	Charlot et al. (2010)	J/AJ/139/1713
33P	33P	I	1420	1	3	255	49.2	Leahy & Roger (1996)	J/A+AS/115/345
GDP	GDP	I	4850	0.5	0.3	253	13	Gregorini et al. (1994)	J/A+AS/106/1
9C	9C	I	15000	0.42	25	242	77.8	Waldram et al. (2003)	J/MNRAS/342/915
5C13	5C13	I	408	1.5	12	238	72.4	Benn (1995)	J/MNRAS/272/699
PiGSS-EN1	PiGSS-EN1	-	3040	1.6	0.15	238	62.3	Croft et al. (2013)	J/ApJ/762/93
5C7	5C7	I	408	1.5	10	235	56.8	Pearson & Kus (1978)	J/MNRAS/182/273
FORb	FORb	S	4750	2.71	25	227	97.4	Forkert & Altschuler (1987)	VIII/57
FORa	FORa	S	2695	4.78	20	221	96.4	Forkert & Altschuler (1987)	VIII/57
WSTB32W	WSTB32W	I	1400	1.2	10	215	40.7	Fanti et al. (1981)	J/A+AS/43/1
5C5	5C5	I	408	1.5	10	214	70.2	Pearson (1975)	J/MNRAS/171/475
[FPD2001b]a	[FPD2001b]a	-	4860	0.0067	0.3	213	37.4	Fanti et al. (2001)	J/A+A/369/380
[MLC2010]	[MLC2010]	I	31000	0.055	0.15	209	24.8	Muchovej et al. (2010)	J/ApJ/716/521
[CCH85]	[CCH85]	I	1411	0.333	5	208	35.9	Coleman et al. (1985)	J/AJ/90/1437
[GPB2012]	[GPB2012]GMRT	I	150	0.4	2	206	47.3	Ghosh et al. (2012)	J/MNRAS/426/3295
[FHW95]d	[FHW95]d	S	8550	2.7	20	205	48.5	Filipovic et al. (1995)	J/A+AS/111/311
[NKB95]	[NKB95]	S	10550	1.15	3	202	65	Niklas et al. (1995)	J/A+AS/114/21
[BI2006]a	[BI2006]a	I	1400	0.02	0.01	200	1.5	Biggs & Ivison (2006)	J/MNRAS/371/963
[FPD2001b]b	[FPD2001b]b	-	8460	0.0033	0.2	199	32.5	Fanti et al. (2001)	J/A+A/369/380
[KFM2008]48	[KFM2008]48	I	4800	0.058	0.01	199	4	Kellermann et al. (2008)	J/ApJS/179/71
KR	KR	I	4890	0.066	10	195	45.4	Fich (1986)	J/AJ/92/787
PiGSS-NDWFS	PiGSS-NDWFS	-	3040	1.6	0.5	195	83.7	Croft et al. (2013)	J/ApJ/762/93
[FHW95]a	[FHW95]a	S	1400	15.2	40	192	51.8	Filipovic et al. (1995)	J/A+AS/111/311
PiGSS-L	PiGSS-L	-	3040	1.6	0.35	189	76.8	Croft et al. (2013)	J/ApJ/762/93
PiGSS-C	PiGSS-C	-	3040	1.6	0.45	186	58.8	Croft et al. (2013)	J/ApJ/762/93
Slee	Slee	I	4900	0.667	0.2	177	34.8	Slee et al. (1996)	VIII/50
[QC93]	[QC93]	S	1410	10	400	171	64	Quiniento & Cersosimo (1993)	J/A+AS/97/435
[HFT2009]8	[HFT2009]8	S	8400	2.4	10.3	156	35	Healey et al. (2009)	J/AJ/138/1032
[SSI2009]330	[SSI2009]330	I	330	0.08	13	150	65.6	Sirothia et al. (2009b)	J/MNRAS/392/1403
CGPSEb	CGPSEa	I	408	3	10	140	29.1	Kerton et al. (2007)	J/MNRAS/379/289
CGPSEa	CGPSEb	I	1420	1	3	140	31.9	Kerton et al. (2007)	J/MNRAS/379/289
[FBR2002]b	[FBR2002]b	I	4800	0.5	1	75	40.8	Filipović et al. (2002)	J/MNRAS/335/1085
[FBR2002]c	[FBR2002]c	I	8640	0.27	1	54	36.4	Filipović et al. (2002)	J/MNRAS/335/1085
37W	37W	I	1400	0.6	1	53	46.3	Walterbos et al. (1985)	J/A+AS/61/451

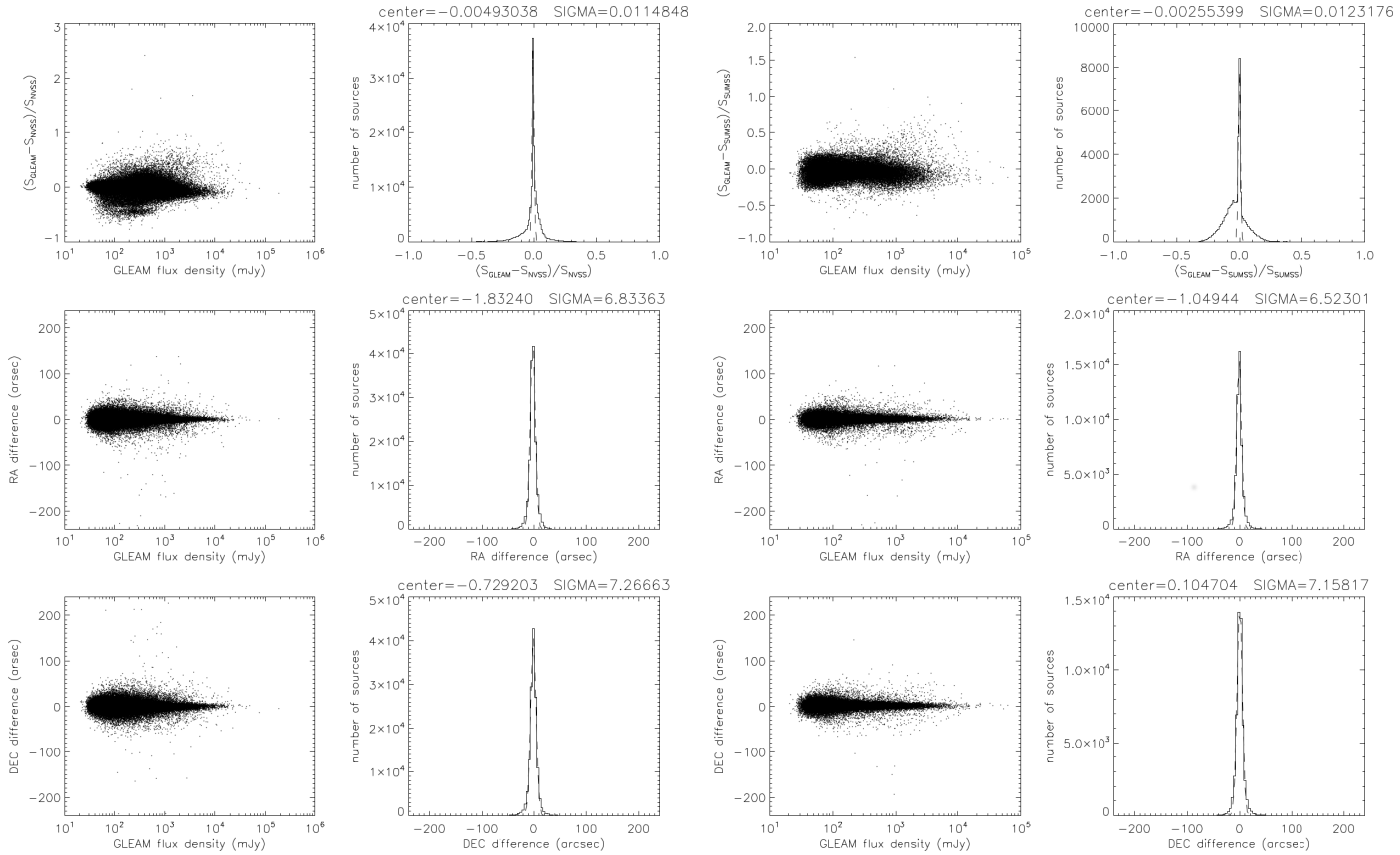

Fig. A.2: Positional and wideband flux density accuracy of the GLEAM survey with respect to the reference, which is the NVSS (left panels) and SUMSS (right panels) for position and the value predicted by the composite spectrum from SPECFIND for the flux density. Upper panel: flux density, middle panel: position offset in right ascension, lower panel: position offset in declination. Right hand panels: solid line: observations, dashed line: fitted Gaussian. The corresponding plots for the other catalogs can be found in the online version of this article. The catalogs are sorted by ascending frequency.

Appendix B: Spectral break, GPS, and MPS sources

To identify spectral break source candidates, we divided the sample of catalog tables into two frequency parts to fit individual spectral slopes to each side of the turnover frequency. We created two catalog subsamples, one subsample below and one subsample above a selected frequency cut. The corresponding frequency of the cut is included in both subsamples to allow for cross-identification. The SPECFIND tool was applied on these subsamples individually. The two complementary spectra of the two subsamples were then combined into one object if they contained the same flux density measurement at the common frequency. The condition for the source classification can be found in Sect. 5.

Appendix B.1: Spectral break sources with peaks around 1.4 GHz

We let the SPECFIND tool find a spectral break around 1.4 GHz by dividing the sample of catalog tables into 128 catalog tables containing frequencies ≤ 1.4 GHz and 125 catalog tables containing frequencies ≥ 1.4 GHz. The overlapping catalog of both subsamples was mostly the NVSS. By doing so, we found a total number of 3104 sources with a spectral break:

(1) 2908 spectral break source candidates
(2) 110 concave spectrum source candidates
(3) 86 GPS source candidates

The 3104 spectral break source candidates have a median and semi-inter-quartile-range (SIQR) value of $\alpha_{\rm high} = -0.83 \pm 0.54$ on the higher-frequency range and $\alpha_{\rm low} = -0.34 \pm 0.74$ on the lower-frequency range. Since the convex sources were removed from the sample, the difference of the medians $\alpha_{\rm high} - \alpha_{\rm low} = -0.49$ is smaller than zero. Whereas the median slope at high frequencies is consistent with the mean slope obtained over the full frequency range (Vollmer et al. 2005a), the slope at low-frequencies is significantly flatter.

In Fig. B.1 we present the high and low-frequency spectral slopes of the entire two subsamples against each other, which means the spectral indices of the higher-frequency subsample ($\alpha_{\rm high}$) as a function of the spectral indices of the low-frequency subsample ($\alpha_{\rm low}$). Most of the spectral indices are located around the one-to-one relation and thus the spectral slopes of both halves of the spectrum are consistent with each other. We provide 15 examples of the 196 sources (from the marked region) in Tab. B.1 along with image cutouts (Fig. B.2). The full list of 3104 spectral break sources is available via the VizieR database.

Finally we show an example of the SPECFIND result for the GPS source candidates NVSS J133600+743755 compared to the result of a query for this source in the VizieR Photometry viewer[9] (Fig. B.3) being consistent with our result. The VizieR Photometry viewer plots all of the available photometric data points extracted from photometry-enabled catalogs in VizieR that fall within a given angular distance of a source position. It covers a much wider frequency range than considered for SPECFIND because it includes catalogs with measurements in other wavebands. The data shown in the Photometry viewer are converted automatically to consistent units using characterization metadata of the magnitude and flux density columns in

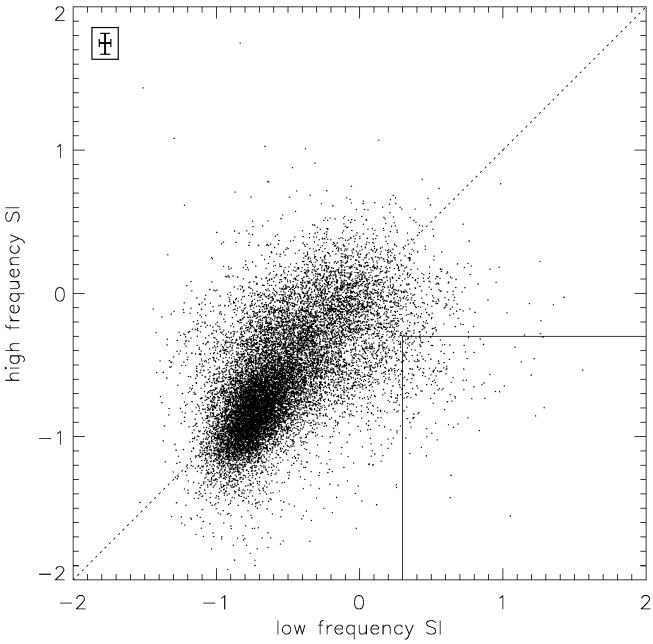

Fig. B.1: Spectral slopes of the subsamples with a frequency cut at 1.4 GHz, including 16 647 sources with and without spectral breaks. The low-frequency spectral slope is on the x-axis, the high-frequency spectral slope is on the y-axis. The diagonal line is the one-to-one relation. Most of the spectral indices are located around the one-to-one relation and thus the spectral slopes of both halves of the spectrum are consistent with each other. The square marks the classification range of concave and GPS source candidates. 196 sources (110 concave and 86 GPS source candidates) fall in this range. The mean error for all points is indicated in the upper left corner.

VizieR tables, which are attached to the proper photometry filter and system (Allen et al. 2014). This automatic extraction of photometry measurements within a radius is different to the more detailed selection criteria and cross matching provided by SPECFIND (as described in section 3). The result shown in the Photometry viewer provides a useful independent check, and the interactive viewer provides a way to explore how the radio data points compare to other wavebands. The example shown uses a 10" radius for the query, and we see that the Photometry viewer results for the radio frequency data points are in accordance with the SPECFIND V3.0 results.

[9] a service available from the VizieR main page, http://vizier.u-strasbg.fr/vizier/sed/ and also integrated in to the CDS Portal http://cdsportal.u-strasbg.fr

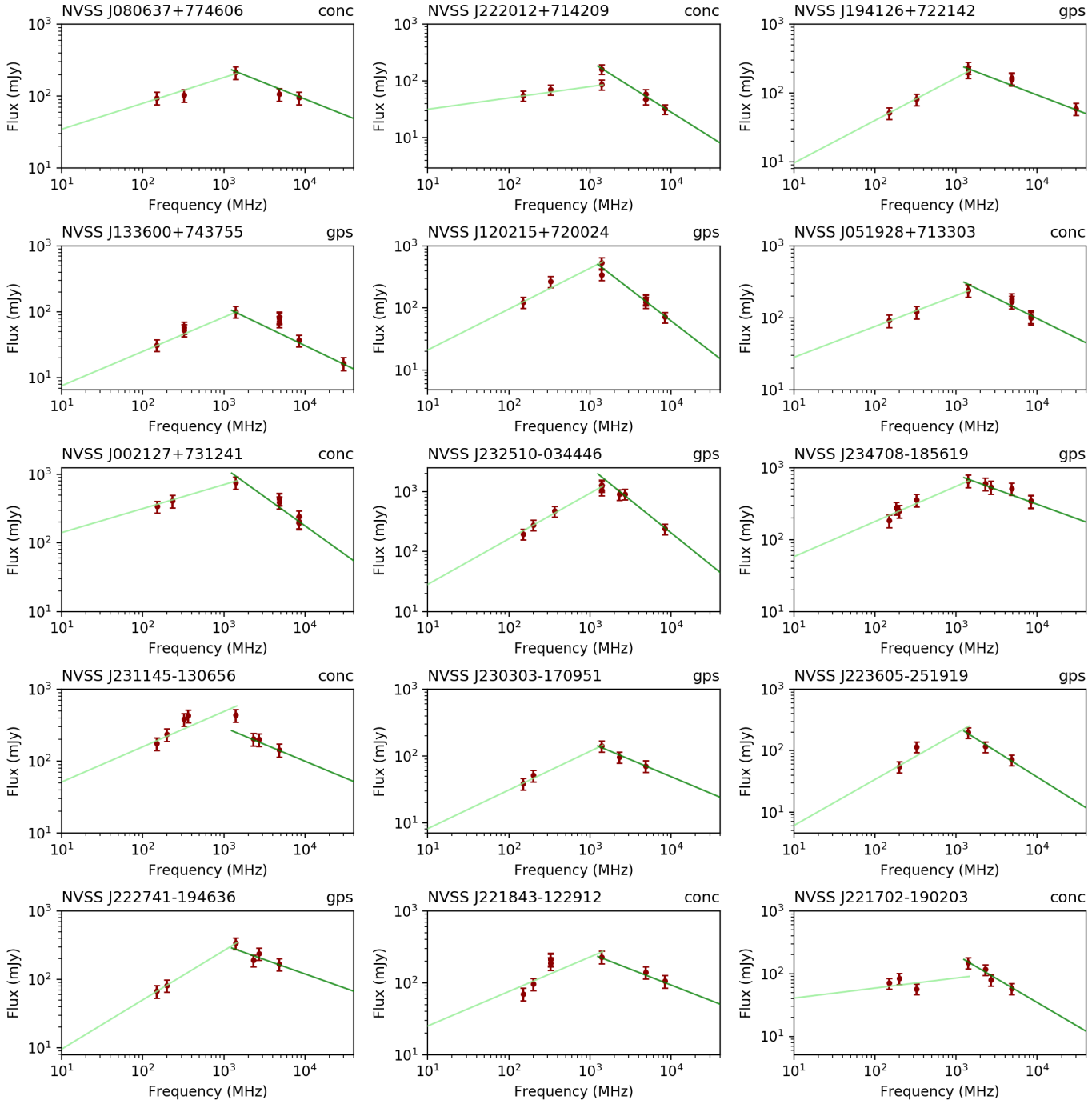

Fig. B.2: Gallery of PS sources in our sample. The title of each spectrum shows the source name and its classification: conc: concave or gps: gigahertz-peaked spectrum sources. See Table B.1 for the list of sources in each of the 15 spectra. More sources are included in the online material.

Table B.1: Concave and GPS sources at 1.4 GHz shown in Fig. B.2.

No	Name	class	α	b	α_{low}	_er	α_{high}	_er	Freq (MHz)	S (mJy)	S_e (mJy)	RA (deg)	Dec (deg)	res (arcmin)
10	WN B0759.6+7754	conc	0.36	1.18	0.38	0.13	-0.47	0.16	325	103.0	21.0	121.6609	77.769	0.2
10	NVSS J080637+774606	conc	0.36	1.18	0.38	0.13	-0.47	0.16	1400	214.0	43.0	121.656	77.7686	0.75
10	TGSSADR J080637.7+774609	conc	0.36	1.18	0.38	0.13	-0.47	0.16	150	94.8	19.0	121.6573	77.7692	0.417
10	[HFT2009]4 J0806+7746	conc	-0.45	3.76	0.38	0.13	-0.47	0.16	4850	107.0	21.0	121.656	77.7686	2.4
10	[HFT2009]8 J080637.404+774607.27	conc	-0.45	3.76	0.38	0.13	-0.47	0.16	8400	94.9	19.0	121.6559	77.7687	2.4
18	WN B2219.0+7127	conc	0.2	1.3	0.35	0.11	-0.9	0.15	325	71.0	14.0	335.0547	71.7033	0.2

No	Name	class	α	b	α_{low}	_er	α_{high}	_er	Freq (MHz)	S (mJy)	S_e (mJy)	RA (deg)	Dec (deg)	res (arcmin)
18	NVSS J222012+714209	conc	0.2	1.3	0.35	0.11	-0.9	0.15	1400	87.5	18.0	335.0509	71.7027	0.75
18	WB 2219+7127	conc	0.48	0.7	0.35	0.11	-0.9	0.15	1400	162.0	32.0	335.0663	71.7022	2.0
18	TGSSADR J222011.9+714208	conc	0.2	1.3	0.35	0.11	-0.9	0.15	150	55.4	11.0	335.0496	71.7024	0.417
18	GB6 B2219+7127	conc	-0.9	5.05	0.35	0.11	-0.9	0.15	4850	48.0	9.6	335.0487	71.7031	5.2
18	87GB 221906.6+712653	conc	-0.9	5.05	0.35	0.11	-0.9	0.15	4850	58.8	12.0	335.0642	71.7	2.3
18	CLASS J222012.1216+714209.903	conc	-0.9	5.05	0.35	0.11	-0.9	0.15	8400	32.1	6.4	335.0505	71.7028	0.0055
25	WN B1942.0+7214	gps	0.62	0.36	0.66	0.1	-0.41	0.08	325	81.0	16.0	295.3593	72.3624	0.2
25	NVSS J194126+722142	gps	0.68	0.23	0.66	0.1	-0.41	0.08	1400	233.0	47.0	295.3624	72.3618	0.75
25	WB 1942+7214	gps	0.62	0.36	0.66	0.1	-0.41	0.08	1400	204.0	41.0	295.3625	72.3603	2.0
25	TGSSADR J194126.7+722142	gps	0.62	0.36	0.66	0.1	-0.41	0.08	150	51.1	10.0	295.3615	72.3617	0.417
25	GB6 B1942+7214	gps	-0.45	3.77	0.66	0.1	-0.41	0.08	4850	165.0	33.0	295.3567	72.3589	1.8
25	87GB 194202.1+721428	gps	-0.45	3.77	0.66	0.1	-0.41	0.08	4850	164.0	33.0	295.3621	72.3606	2.3
25	BWE 1942+7214	gps	-0.45	3.77	0.66	0.1	-0.41	0.08	4850	158.0	32.0	295.3625	72.3603	2.3
25	[PGB2011] J1941+7221	gps	-0.45	3.77	0.66	0.1	-0.41	0.08	30000	59.3	12.0	295.3625	72.3617	1.2
34	WN B1335.0+7453m	gps	0.52	0.36	0.5	0.12	-0.64	0.1	325	53.0	11.0	204.0006	74.6322	0.2
34	WN B1335.0+7453p	gps	0.52	0.36	0.5	0.12	-0.64	0.1	325	58.0	12.0	203.9987	74.6312	0.2
34	NVSS J133600+743755	gps	0.52	0.36	0.5	0.12	-0.64	0.1	1400	101.0	20.0	204.0007	74.6319	0.75
34	TGSSADR J133559.7+743755	gps	0.52	0.36	0.5	0.12	-0.64	0.1	150	31.4	6.3	203.9991	74.632	0.417
34	GB6 B1335+7453	gps	-0.64	4.07	0.5	0.12	-0.64	0.1	4850	72.0	14.0	203.9917	74.635	1.8
34	87GB 133501.0+745315	gps	-0.64	4.07	0.5	0.12	-0.64	0.1	4850	84.0	17.0	203.9817	74.6331	2.3
34	BWE 1335+7453	gps	-0.64	4.07	0.5	0.12	-0.64	0.1	4850	80.0	16.0	203.9825	74.6336	2.3
34	CLASS J133600.2313+743754.719	gps	-0.59	3.85	0.5	0.12	-0.64	0.1	8400	37.3	7.5	204.001	74.6319	0.0055
34	[PGB2011] J1336+7437	gps	-0.59	3.85	0.5	0.12	-0.64	0.1	30000	16.6	3.8	204.0008	74.6319	1.2
34	CRATES J133558+743806	gps	-0.59	3.85	0.5	0.12	-0.64	0.1	8400	37.3	7.5	204.001	74.6319	0.1
35	WN B1159.7+7217	gps	0.66	0.66	0.51	0.11	-0.98	0.12	325	268.0	54.0	180.5635	72.0068	0.2
35	NVSS J120215+720024	gps	0.52	0.98	0.51	0.11	-0.98	0.12	1400	344.0	69.0	180.564	72.0069	0.75
35	WB 1159+7216	gps	0.66	0.66	0.51	0.11	-0.98	0.12	1400	537.0	110.0	180.5625	72.0039	2.0
35	TGSSADR J120215.3+720024	gps	0.66	0.66	0.51	0.11	-0.98	0.12	150	124.0	25.0	180.5638	72.0068	0.417
35	GB6 B1159+7216	gps	-1.01	5.83	0.51	0.11	-0.98	0.12	4850	124.0	25.0	180.5642	72.0044	1.8
35	87GB 115942.6+721656	gps	-1.13	6.28	0.51	0.11	-0.98	0.12	4850	140.0	28.0	180.5646	72.0039	2.3
35	BWE 1159+7216	gps	-1.13	6.28	0.51	0.11	-0.98	0.12	4850	135.0	27.0	180.5625	72.0039	2.3
35	CLASS J120215.3413+720024.609	gps	-1.01	5.83	0.51	0.11	-0.98	0.12	8400	71.0	14.0	180.5639	72.0068	0.0055
55	WN B0513.6+7129	conc	0.43	1.02	0.44	0.1	-0.46	0.1	325	121.0	24.0	79.8681	71.5519	0.2
55	NVSS 051928+713303	conc	0.44	1.01	0.44	0.1	-0.46	0.1	1400	243.0	49.0	79.8702	71.5511	0.75
55	WB J513+7129	conc	0.43	1.02	0.44	0.1	-0.46	0.1	1400	241.0	48.0	79.8692	71.5522	2.0
55	TGSSADR J051928.3+713302	conc	0.43	1.02	0.44	0.1	-0.46	0.1	150	91.7	18.0	79.8682	71.5508	0.417
55	GB6 B0513+7129	conc	-0.56	4.23	0.44	0.1	-0.46	0.1	4850	167.0	33.0	79.8688	71.5492	1.8
55	87GB J51338.3+712959	conc	-0.47	3.86	0.44	0.1	-0.46	0.1	4850	181.0	36.0	79.8683	71.5522	2.3
55	JVAS J0519+715	conc	-0.49	3.93	0.44	0.1	-0.46	0.1	8400	100.0	20.0	79.8703	71.551	0.0055
55	CLASS J051928.8852+713303.745	conc	-0.56	4.23	0.44	0.1	-0.46	0.1	8400	105.0	21.0	79.8703	71.551	0.0055
55	CRATES J051928+713257	conc	-0.56	4.23	0.44	0.1	-0.46	0.1	8400	105.0	21.0	79.8704	71.551	0.1
65	NVSS J002127+731241	conc	0.35	1.8	0.36	0.12	-0.73	0.13	1400	763.0	150.0	5.3642	73.2115	0.75
65	MY 001830.9+731242.9	conc	0.35	1.8	0.36	0.12	-0.73	0.13	232	410.0	85.0	5.3492	73.2119	2.5
65	6C J01831+725602	conc	0.35	1.8	0.36	0.12	-0.73	0.13	151	340.0	68.0	5.3508	73.2111	4.2
65	GB6 B0018+7256	conc	-0.85	5.65	0.36	0.12	-0.73	0.13	4850	438.0	88.0	5.3688	73.2111	1.8
65	87GB 001835.0+725604	conc	-0.85	5.65	0.36	0.12	-0.73	0.13	4850	441.0	88.0	5.3662	73.2117	2.3
65	BWE 0018+7256	conc	-0.85	5.65	0.36	0.12	-0.73	0.13	4850	393.0	79.0	5.3667	73.2119	2.3
65	JVAS J0021+732	conc	-0.85	5.65	0.36	0.12	-0.73	0.13	8400	196.0	39.0	5.3641	73.2116	0.0055
65	CLASS J002127.3751+731241.929	conc	-0.63	4.88	0.36	0.12	-0.73	0.13	8400	245.0	49.0	5.364	73.2116	0.0055
65	CLASS J002127.3782+731241.902	conc	-0.85	5.65	0.36	0.12	-0.73	0.13	8400	204.0	41.0	5.364	73.2116	0.0055
93	TXS 2322-040	gps	0.76	0.69	0.76	0.09	-0.87	0.13	365	472.0	94.0	351.2932	-3.7464	0.1
93	NVSS J232510-034446	gps	0.76	0.69	0.76	0.09	-0.87	0.13	1400	1220.0	240.0	351.2926	-3.7463	0.75
93	TGSSADR J232510.2-034446	gps	0.82	0.51	0.76	0.09	-0.87	0.13	150	196.0	39.0	351.2928	-3.7462	0.417
93	GLEAM J232509-034450	gps	0.76	0.69	0.76	0.09	-0.87	0.13	200	277.0	55.0	351.2915	-3.7473	2.0
93	FIRST14 J232510.2-034446	gps	0.69	0.86	0.76	0.09	-0.87	0.13	1400	1060.0	210.0	351.2926	-3.7462	0.0833
93	PKS J2325-0344	gps	-1.02	6.37	0.76	0.09	-0.87	0.13	2700	910.0	180.0	351.2933	-3.745	1.0
93	WB 2322-0401	gps	-1.02	6.37	0.76	0.09	-0.87	0.13	1400	1290.0	260.0	351.3104	-3.7536	2.0
93	SPASS J232510-034437	gps	-0.91	5.95	0.76	0.09	-0.87	0.13	2307	894.0	180.0	351.2933	-3.7437	10.75
93	PKS8400 J2325-0344	gps	-1.09	6.67	0.76	0.09	-0.87	0.13	8400	240.0	48.0	351.2933	-3.745	2.7
115	WISH B2344.5-1913	gps	0.49	1.27	0.51	0.11	-0.36	0.12	325	355.0	71.0	356.7854	-18.9388	0.3
115	NVSS J234708-185619	gps	0.49	1.27	0.51	0.11	-0.36	0.12	1400	655.0	130.0	356.7861	-18.9386	0.75
115	TGSSADR J234708.5-185618	gps	0.49	1.27	0.51	0.11	-0.36	0.12	150	184.0	37.0	356.7857	-18.9385	0.417

No	Name	class	α	b	α_{low}	_er	α_{high}	_er	Freq (MHz)	S (mJy)	S_e (mJy)	RA (deg)	Dec (deg)	res (arcmin)
115	GLEAM J234708-185615	gps	0.49	1.27	0.51	0.11	-0.36	0.12	200	251.0	50.0	356.7865	-18.9377	2.0
115	KGS J234709-185632	gps	0.42	1.49	0.51	0.11	-0.36	0.12	182	276.0	55.0	356.7902	-18.9423	0.04
115	PMN J2347-1856	gps	-0.39	4.07	0.51	0.11	-0.36	0.12	4850	512.0	100.0	356.7879	-18.9419	2.8
115	PKS J2347-1856	gps	-0.41	4.13	0.51	0.11	-0.36	0.12	2700	540.0	110.0	356.7858	-18.9383	1.0
115	SPASS J234706-185606	gps	-0.39	4.07	0.51	0.11	-0.36	0.12	2307	601.0	120.0	356.7772	-18.935	10.75
115	CRATES J234709-185631	gps	-0.39	4.07	0.51	0.11	-0.36	0.12	8400	347.0	69.0	356.786	-18.9386	0.1
115	PKS8400 J2347-1856	gps	-0.41	4.13	0.51	0.11	-0.36	0.12	8400	340.0	68.0	356.786	-18.9385	2.7
128	TXS 2309-133	conc	0.49	1.22	0.37	0.12	-0.87	0.23	365	433.0	87.0	347.9415	-13.1146	0.1
128	WISH B2309.1-1323	conc	0.32	1.65	0.37	0.12	-0.87	0.23	325	386.0	77.0	347.941	-13.1149	0.3
128	NVSS J231145-130656	conc	0.32	1.65	0.37	0.12	-0.87	0.23	1400	437.0	87.0	347.9409	-13.1156	0.75
128	TGSSADR J231146.0-130653	conc	0.32	1.65	0.37	0.12	-0.87	0.23	150	177.0	35.0	347.9417	-13.115	0.417
128	GLEAM J231145-130705	conc	0.32	1.65	0.37	0.12	-0.87	0.23	200	237.0	47.0	347.9411	-13.1182	2.0
128	PMN J2311-1306	conc	-0.47	3.88	0.37	0.12	-0.87	0.23	4850	144.0	29.0	347.94	-13.1125	2.8
128	PKS J2311-1307	conc	-0.47	3.88	0.37	0.12	-0.87	0.23	2700	200.0	40.0	347.9404	-13.1228	1.0
128	SPASS J231144-130620	conc	-0.47	3.88	0.37	0.12	-0.87	0.23	2307	204.0	41.0	347.9352	-13.1056	10.75
133	NVSS J230303-170951	gps	0.58	0.33	0.56	0.12	-0.55	0.23	1400	142.0	28.0	345.7646	-17.1643	0.75
133	TGSSADR J230303.4-170952	gps	0.58	0.33	0.56	0.12	-0.55	0.23	150	38.9	7.8	345.7643	-17.1646	0.417
133	GLEAM J230304-170957	gps	0.58	0.33	0.56	0.12	-0.55	0.23	200	51.2	10.0	345.7674	-17.1661	2.0
133	PMN J2303-1709	gps	-0.64	4.16	0.56	0.12	-0.55	0.23	4850	71.0	14.0	345.7683	-17.1639	2.8
133	SPASS J230303-170915	gps	-0.51	3.73	0.56	0.12	-0.55	0.23	2307	96.8	19.0	345.7646	-17.1544	10.75
146	WISH B2233.3-2534	gps	0.75	0.03	0.59	0.14	-0.81	0.23	325	116.0	23.0	339.0232	-25.3172	0.3
146	NVSS J223605-251919	gps	0.75	0.03	0.59	0.14	-0.81	0.23	1400	198.0	40.0	339.0244	-25.3222	0.75
146	GLEAM J223605-251922	gps	0.75	0.03	0.59	0.14	-0.81	0.23	200	54.8	11.0	339.0228	-25.3229	2.0
146	PMN J2236-2519	gps	-0.83	4.89	0.59	0.14	-0.81	0.23	4850	71.0	14.0	339.03	-25.3247	2.8
146	SPASS J223608-252117	gps	-0.83	4.89	0.59	0.14	-0.81	0.23	2307	117.0	23.0	339.036	-25.3549	10.75
149	NVSS J222741-194636	gps	0.72	0.26	0.73	0.12	-0.53	0.23	1400	340.0	68.0	336.9228	-19.7767	0.75
149	TGSSADR J222741.3-194636	gps	0.72	0.26	0.73	0.12	-0.53	0.23	150	67.6	14.0	336.9222	-19.7767	0.417
149	GLEAM J222741-194633	gps	0.72	0.26	0.73	0.12	-0.53	0.23	200	81.9	16.0	336.9244	-19.776	2.0
149	PMN J2227-1946	gps	-0.57	4.31	0.73	0.12	-0.53	0.23	4850	168.0	34.0	336.92	-19.7772	2.8
149	PKS J2227-1946	gps	-0.57	4.31	0.73	0.12	-0.53	0.23	2700	240.0	48.0	336.9175	-19.7808	1.0
149	SPASS J222741-194644	gps	-0.42	3.76	0.73	0.12	-0.53	0.23	2307	190.0	38.0	336.924	-19.779	10.75
151	WISH B2216.0-1244a	conc	0.48	0.92	0.48	0.12	-0.43	0.16	325	215.0	43.0	334.6807	-12.4922	0.3
151	WISH B2216.0-1244A	conc	0.48	0.92	0.48	0.12	-0.43	0.16	325	187.0	37.0	334.6802	-12.4872	0.3
151	WISH B2216.0-1244b	conc	0.48	0.92	0.48	0.12	-0.43	0.16	325	209.0	42.0	334.6811	-12.4857	0.3
151	NVSS J221843-122912	conc	0.48	0.92	0.48	0.12	-0.43	0.16	1400	230.0	46.0	334.6812	-12.4869	0.75
151	TGSSADR J221843.3-122912	conc	0.53	0.69	0.48	0.12	-0.43	0.16	150	70.2	14.0	334.6808	-12.4869	0.417
151	GLEAM J221843-122916	conc	0.53	0.69	0.48	0.12	-0.43	0.16	200	96.8	19.0	334.682	-12.4879	2.0
151	PMN J2218-1229	conc	-0.44	3.73	0.48	0.12	-0.43	0.16	4850	141.0	28.0	334.6846	-12.485	2.8
151	CRATES J221844-122906	conc	-0.44	3.73	0.48	0.12	-0.43	0.16	8400	106.0	21.0	334.681	-12.487	0.1
152	WISH B2214.3-1916	conc	0.16	1.45	0.33	0.12	-0.79	0.23	325	57.0	11.0	334.2603	-19.0306	0.3
152	NVSS J221702-190203	conc	0.34	1.12	0.33	0.12	-0.79	0.23	1400	150.0	30.0	334.2589	-19.0343	0.75
152	TGSSADR J221702.0-190203	conc	0.34	1.12	0.33	0.12	-0.79	0.23	150	70.8	14.0	334.2586	-19.0343	0.417
152	GLEAM J221702-190207	conc	0.34	1.12	0.33	0.12	-0.79	0.23	200	84.8	17.0	334.2583	-19.0355	2.0
152	PMN J2216-1901	conc	-0.76	4.58	0.33	0.12	-0.79	0.23	4850	58.0	12.0	334.2454	-19.0331	2.8
152	PKS J2217-1901	conc	-0.76	4.58	0.33	0.12	-0.79	0.23	2700	80.0	16.0	334.2579	-19.0322	1.0
152	SPASS J221656-190115	conc	-0.76	4.58	0.33	0.12	-0.79	0.23	2307	117.0	23.0	334.235	-19.021	10.75

Columns: "No" running number with the same number for sources of the same spectrum, "Name" provides the source name. The column "class" gives the type (spectral break (sb), concave (conc), GPS/MPS (gps/mps)). "α" and "b" are the spectral slope and the abscissa of the spectral fit associated with the source. "α_{low}" is the mean spectral slope of the low-frequency part of the spectrum with its error "er," "α_{high}" is the mean spectral slope of the high-frequency part of the spectrum with its error "er." "Freq" is the frequency, "S" the flux density and "S_e" its error. Lastly, the position (Right Ascension and Declination) and "res" the beam/resolution are specified. The last 6 columns refer to the source and survey given in the column "Name."

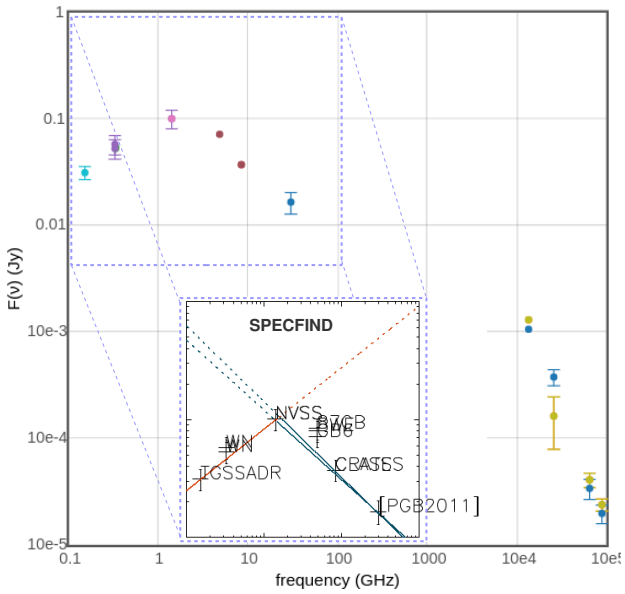

Fig. B.3: Photometric viewer result for the GPS source candidate NVSS J133600+743755 with 10" query radius. The inset correspond to the radio continuum spectrum from SPECFIND V3.0, showing that the Photometry viewer results are in accordance with the SPECFIND V3.0 results.

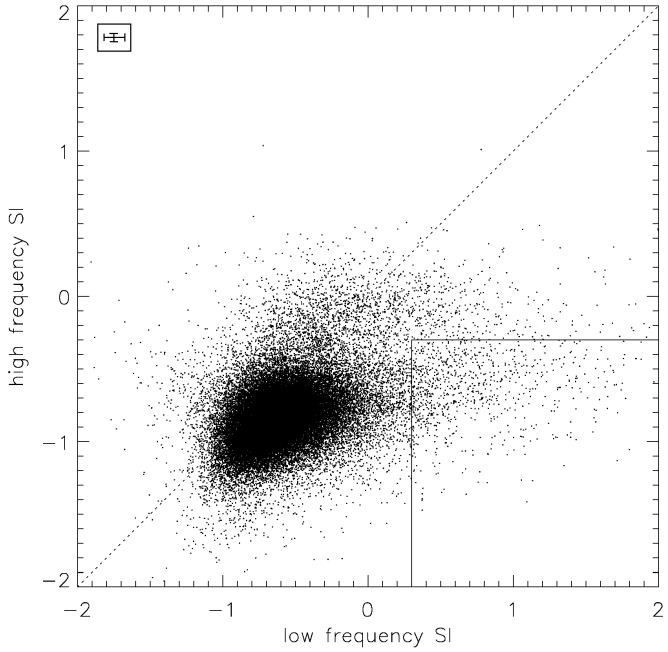

Fig. B.4: Spectral slopes of the subsamples with a frequency cut at 325 MHz, including 48535 sources with and without spectral breaks. The low-frequency spectral slope is on the x-axis, the high-frequency spectral slope is y-axis. The diagonal line is the one-to-one relation. Most of the spectral indices are slightly below the one-to-one relation. The entire sample shows a median and semi-inter-quartile-range (SIQR) value of the spectral slope of $\alpha_{\rm high} = -0.83 \pm 0.24$ on the higher-frequency part and $\alpha_{\rm low} = -0.61 \pm 0.31$ on the lower-frequency part. The square marks the classification range of concave source candidates. In this region, 874 sources (327 concave and 547 MPS source candidates) are located. The mean error for all points is indicated in the upper left corner.

Appendix B.2: Spectral break sources with peaks around 325 MHz

We let the SPECFIND tool find a spectral break around 325 MHz by dividing the sample of catalog tables into two subsamples. The first subsample contains 51 catalog tables with frequencies $\leq$ 325 MHz and the second subsample contains 168 catalog tables with frequencies $\geq$ 325 MHz. The overlapping catalogs are often the Texas Survey (TXS, Douglas et al. 1996), the Westerbork Northern Sky Survey (WENSS, Rengelink et al. 1997) or the Westerbork In the Southern Hemisphere (WISH, De Breuck et al. 2002). By doing so, we found a total number of 18 075 sources with a spectral break:

(1) 17 201 spectral break source candidates
(2) 327 concave source candidates
(3) 547 MPS source candidates

All 18 075 spectral break source candidates have a median and SIQR of the spectral slope of $\alpha_{\rm high} = -0.88 \pm 0.26$ on the higher-frequency part and $\alpha_{\rm low} = -0.44 \pm 0.35$ on the lower-frequency part. These numbers are consistent with those obtained for the sources with breaks at 1.4 GHz. In Figure B.4 we present the high and low-frequency spectral slopes of the two subsamples plotted against each other of all sources, which means, the spectral indices of the subsample $\geq$ 325 MHz against the ones of the $\leq$ 325 MHz frequency subsample. The median and SIQR of the spectral slope are $\alpha_{\rm high} = -0.83 \pm 0.24$ at high frequencies and $\alpha_{\rm low} = -0.61 \pm 0.31$ at low frequencies. For comparison, the median GLEAM spectral index is significantly steeper $\alpha = -0.8 \pm 0.1$ (Hurley-Walker et al. 2017b). As stated in Sects. 4.3 and 5, the apparent flattening of the spectral index at low frequencies is caused by (i) contamination by systematics and (ii) our selection bias for source with low flux densities at low frequencies (see Fig. 2). This leads to a contamination of our PS source candidate sample.

We present 15 examples of the 874 PS source candidates (within the marked region) in the appendix Tab. B.2 along with image cutouts in appendix Fig. B.5. The full table of all 18 075 spectral break source candidates is available via the VizieR database.

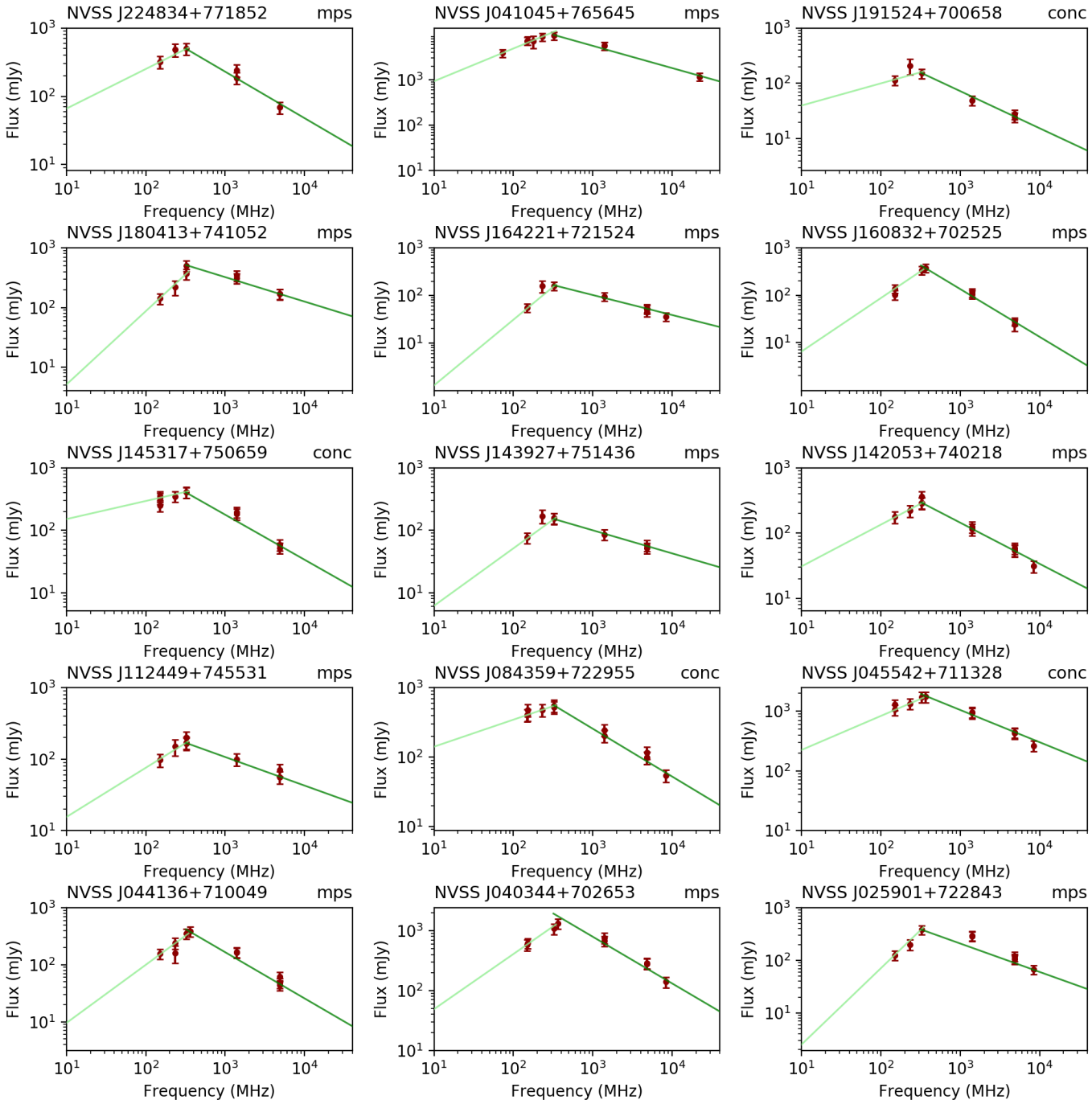

Fig. B.5: Gallery of megahertz-peaked spectrum sources in our sample. The title of each spectrum shows the source name and its classification: conc: concave spectrum source or mps: megahertz-peaked spectrum source. See Table B.2 for the list of sources in each of the 15 spectra. More sources are included in the online material.

Table B.2: Concave and MPS sources at 325 MHz shown in Fig. B.5.

No	Name	class	α	b	α_{low}	_er	α_{high}	_er	Freq (MHz)	S (mJy)	S_e (mJy)	RA (deg)	Dec (deg)	res (arcmin)
3	WN B2247.5+7702	mps	0.58	1.24	0.6	0.37	-0.73	0.11	325	501.0	100.0	342.1472	77.3137	0.2
3	MY 224745.5+771849.2	mps	0.58	1.24	0.6	0.37	-0.73	0.11	232	480.0	100.0	342.2038	77.3137	2.5
3	TGSSADR J224834.2+771846	mps	0.58	1.24	0.6	0.37	-0.73	0.11	150	320.0	64.0	342.1426	77.313	0.417
3	NVSS J224834+771852	mps	-0.76	4.65	0.6	0.37	-0.73	0.11	1400	240.0	48.0	342.1452	77.3146	0.75
3	WB 2247+7703	mps	-0.73	4.55	0.6	0.37	-0.73	0.11	1400	186.0	37.0	342.1171	77.3194	2.0
3	[HFT2009]4 J2248+7718	mps	-0.68	4.4	0.6	0.37	-0.73	0.11	4850	68.7	14.0	342.1452	77.3145	2.4
23	4C +76.03	mps	0.72	2.25	0.6	0.18	-0.51	0.07	178	7100.0	2100.0	62.68	76.9133	11.5

No	Name	class	α	b	α_{low}	_er	α_{high}	_er	Freq (MHz)	S (mJy)	S_e (mJy)	RA (deg)	Dec (deg)	res (arcmin)
23	WN B0403.9+7648	mps	0.72	2.25	0.6	0.18	-0.51	0.07	325	9410.0	1900.0	62.6897	76.9457	0.2
23	MY 040401.5+765638.5	mps	0.72	2.25	0.6	0.18	-0.51	0.07	232	8920.0	1800.0	62.6996	76.944	2.5
23	6C 040359+764849	mps	0.72	2.25	0.6	0.18	-0.51	0.07	151	7350.0	1500.0	62.6925	76.945	4.2
23	TGSSADR J041045.4+765645	mps	0.72	2.25	0.6	0.18	-0.51	0.07	150	7180.0	1400.0	62.6894	76.946	0.417
23	VLSSr J041042.3+765642	mps	0.72	2.25	0.6	0.18	-0.51	0.07	73	3920.0	780.0	62.6766	76.9451	1.25
23	NVSS J041045+765645	mps	-0.49	5.22	0.6	0.18	-0.51	0.07	1400	5620.0	1100.0	62.6901	76.9459	0.75
23	WB 0403+7648	mps	-0.49	5.22	0.6	0.18	-0.51	0.07	1400	5670.0	1100.0	62.6846	76.9417	2.0
23	K-RFC J0410+7656	mps	-0.49	5.22	0.6	0.18	-0.51	0.07	22000	1170.0	230.0	62.6901	76.9459	2.1
125	WN B1915.7+7001	conc	0.4	1.2	0.39	0.37	-0.64	0.09	325	152.0	30.0	288.8492	70.115	0.2
125	MY 191538.5+700713.1	conc	0.36	1.27	0.39	0.37	-0.64	0.09	232	210.0	68.0	288.8246	70.1203	2.5
125	TGSSADR J191523.9+700701	conc	0.4	1.2	0.39	0.37	-0.64	0.09	150	114.0	23.0	288.8499	70.117	0.417
125	GB6 B1915+7002	conc	-0.67	3.87	0.39	0.37	-0.64	0.09	4850	24.6	4.9	288.8542	70.1261	1.8
125	87GB 191547.3+700237	conc	-0.67	3.87	0.39	0.37	-0.64	0.09	4850	27.8	5.6	288.8613	70.1339	2.3
125	NVSS J191524+700658	conc	-0.67	3.87	0.39	0.37	-0.64	0.09	1400	49.4	9.9	288.8514	70.1164	0.75
143	WN B1805.5+7411B	mps	1.23	-0.52	1.22	0.37	-0.34	0.07	325	369.0	74.0	271.0562	74.1816	0.2
143	MY 180536.5+741057.9	mps	1.23	-0.52	1.22	0.37	-0.34	0.07	232	220.0	61.0	271.0608	74.1828	2.5
143	TGSSADR J180413.8+741051	mps	1.23	-0.52	1.22	0.37	-0.34	0.07	150	143.0	29.0	271.0576	74.181	0.417
143	GB6 B1805+7410	mps	-0.4	3.72	1.22	0.37	-0.34	0.07	4850	169.0	34.0	271.055	74.1828	1.8
143	87GB 180535.2+741041	mps	-0.41	3.74	1.22	0.37	-0.34	0.07	4850	170.0	34.0	271.0554	74.1842	2.3
143	WN B1805.5+7411	mps	-0.4	3.72	1.22	0.37	-0.34	0.07	325	504.0	100.0	271.0547	74.1893	0.2
143	NVSS J180413+741052	mps	-0.29	3.29	1.22	0.37	-0.34	0.07	1400	312.0	62.0	271.0577	74.1813	0.75
143	WB 1805+7410	mps	-0.41	3.74	1.22	0.37	-0.34	0.07	1400	344.0	69.0	271.055	74.1842	2.0
155	WN B1643.0+7220	mps	1.38	-1.27	1.41	0.37	-0.46	0.08	325	160.0	32.0	250.5882	72.2564	0.2
155	MY 164304.2+721547.5	mps	1.38	-1.27	1.41	0.37	-0.46	0.08	232	160.0	44.0	250.5846	72.2632	2.5
155	TGSSADR J164221.7+721523	mps	1.38	-1.27	1.41	0.37	-0.46	0.08	150	55.0	11.0	250.5908	72.2566	0.417
155	GB6 B1643+7221	mps	-0.46	3.35	1.41	0.37	-0.46	0.08	4850	45.0	9.0	250.5708	72.2581	1.8
155	87GB 164300.1+722111	mps	-0.42	3.27	1.41	0.37	-0.46	0.08	4850	51.0	10.0	250.5679	72.2608	2.3
155	BWE 1643+7219	mps	-0.46	3.35	1.41	0.37	-0.46	0.08	4850	54.0	11.0	250.6213	72.2397	2.3
155	NVSS J164221+721524	mps	-0.42	3.27	1.41	0.37	-0.46	0.08	1400	95.9	19.0	250.5891	72.2569	0.75
155	CLASS J164221.5359+721524.664	mps	-0.42	3.27	1.41	0.37	-0.46	0.08	8400	36.1	7.2	250.5897	72.2568	0.0055
158	TXS 1608+705	mps	1.13	-0.32	1.3	0.25	-0.97	0.08	365	379.0	76.0	242.1358	70.4236	0.1
158	WN B1608.7+7033	mps	1.13	-0.32	1.3	0.25	-0.97	0.08	325	337.0	67.0	242.1359	70.4237	0.2
158	7C 160845.89+703310.00	mps	1.36	-0.9	1.3	0.25	-0.97	0.08	151	102.0	23.0	242.1371	70.4228	1.17
158	TGSSADR J160832.5+702521	mps	1.13	-0.32	1.3	0.25	-0.97	0.08	150	139.0	28.0	242.1356	70.4226	0.417
158	GB6 B1608+7033	mps	-1.01	5.16	1.3	0.25	-0.97	0.08	4850	28.0	5.6	242.1354	70.4258	1.8
158	BWE 1608+7033	mps	-1.07	5.31	1.3	0.25	-0.97	0.08	4850	24.0	6.5	242.1433	70.4281	2.3
158	NVSS J160832+702525	mps	-1.01	5.16	1.3	0.25	-0.97	0.08	1400	115.0	23.0	242.136	70.4237	0.75
158	WB 1608+7033	mps	-1.01	5.16	1.3	0.25	-0.97	0.08	1400	104.0	21.0	242.1433	70.4281	2.0
166	WN B1453.6+7519m	conc	0.29	1.89	0.37	0.24	-0.74	0.07	325	407.0	81.0	223.3264	75.1162	0.2
166	WN B1453.6+7519p	conc	0.3	1.86	0.37	0.24	-0.74	0.07	325	411.0	82.0	223.3269	75.1163	0.2
166	MY 145342.2+750638.5	conc	0.45	1.49	0.37	0.24	-0.74	0.07	232	350.0	70.0	223.3425	75.1107	2.5
166	6C 145345+751851	conc	0.45	1.49	0.37	0.24	-0.74	0.07	151	250.0	50.0	223.3546	75.1119	4.2
166	7C 145337.10+751909.00	conc	0.29	1.89	0.37	0.24	-0.74	0.07	151	327.0	65.0	223.3208	75.1167	1.17
166	TGSSADR J145317.8+750657	conc	0.29	1.89	0.37	0.24	-0.74	0.07	150	352.0	70.0	223.3245	75.116	0.417
166	GB6 B1453+7519	conc	-0.72	4.41	0.37	0.24	-0.74	0.07	4850	58.8	12.0	223.3	75.1167	1.8
166	BWE 1453+7519	conc	-0.72	4.41	0.37	0.24	-0.74	0.07	4850	52.0	10.0	223.3038	75.1256	2.3
166	NVSS J145317+750659	conc	-0.72	4.41	0.37	0.24	-0.74	0.07	1400	184.0	37.0	223.3244	75.1166	0.75
166	WB 1453+7519	conc	-0.72	4.41	0.37	0.24	-0.74	0.07	1400	196.0	39.0	223.3038	75.1256	2.0
169	WN B1439.6+7527m	mps	0.92	-0.13	0.89	0.32	-0.39	0.07	325	155.0	31.0	219.8662	75.2429	0.2
169	WN B1439.6+7527p	mps	0.94	-0.16	0.89	0.32	-0.39	0.07	325	157.0	31.0	219.8665	75.2438	0.2
169	MY 143946.6+751516.1	mps	0.92	-0.13	0.89	0.32	-0.39	0.07	232	170.0	42.0	219.9008	75.2545	2.5
169	TGSSADR J143927.5+751436	mps	0.92	-0.13	0.89	0.32	-0.39	0.07	150	76.0	15.0	219.8649	75.2435	0.417
169	GB6 B1439+7527	mps	-0.37	3.11	0.89	0.32	-0.39	0.07	4850	57.5	12.0	219.8383	75.2447	1.8
169	BWE 1439+7527	mps	-0.4	3.21	0.89	0.32	-0.39	0.07	4850	52.0	10.0	219.8487	75.2508	2.3
169	NVSS J143927+751436	mps	-0.37	3.11	0.89	0.32	-0.39	0.07	1400	85.9	17.0	219.8665	75.2435	0.75
174	WN B1420.6+7416	mps	0.64	0.85	0.76	0.29	-0.67	0.05	325	288.0	58.0	215.2282	74.0393	0.2
174	MY 142042.9+740253.0	mps	0.64	0.85	0.76	0.29	-0.67	0.05	232	220.0	44.0	215.2537	74.0481	2.5
174	WSTBa 70W0408*	mps	0.64	0.85	0.76	0.29	-0.67	0.05	327	365.0	73.0	215.2335	74.0395	1.5
174	WSTBa 70W0408A	mps	0.63	0.89	0.76	0.29	-0.67	0.05	327	292.0	58.0	215.2208	74.0384	1.5
174	TGSSADR J142053.0+740218	mps	0.63	0.89	0.76	0.29	-0.67	0.05	150	177.0	35.0	215.2209	74.0386	0.417
174	GB6 B1420+7416	mps	-0.64	4.08	0.76	0.29	-0.67	0.05	4850	54.0	11.0	215.2108	74.0403	1.8
174	87GB 142030.5+741600	mps	-0.64	4.08	0.76	0.29	-0.67	0.05	4850	59.0	12.0	215.2033	74.0392	2.3
174	BWE 1420+7415	mps	-0.63	4.05	0.76	0.29	-0.67	0.05	4850	55.0	11.0	215.1987	74.0386	2.3
174	NVSS J142053+740218	mps	-0.59	3.96	0.76	0.29	-0.67	0.05	1400	125.0	25.0	215.222	74.0385	0.75
174	WB 1420+7415	mps	-0.62	4.02	0.76	0.29	-0.67	0.05	1400	115.0	23.0	215.1987	74.0386	2.0
174	CLASS J142053.1109+740218.785	mps	-0.63	4.05	0.76	0.29	-0.67	0.05	8400	31.1	6.2	215.2213	74.0386	0.0055

No	Name	class	α	b	α_{low}	_er	α_{high}	_er	Freq (MHz)	S (mJy)	S_e (mJy)	RA (deg)	Dec (deg)	res (arcmin)
209	WN B1121.6+7511	mps	0.69	0.5	0.76	0.3	-0.39	0.07	325	166.0	33.0	171.2085	74.9221	0.2
209	WN B1121.5+7512	mps	0.93	-0.04	0.76	0.3	-0.39	0.07	325	201.0	40.0	171.2008	74.9257	0.2
209	WN B1121.5+7512B	mps	0.72	0.41	0.76	0.3	-0.39	0.07	325	171.0	34.0	171.2146	74.9226	0.2
209	MY 112132.2+745509.6	mps	0.93	-0.04	0.76	0.3	-0.39	0.07	232	150.0	38.0	171.1917	74.9193	2.5
209	TGSSADR J112446.9+745546	mps	0.93	-0.04	0.76	0.3	-0.39	0.07	150	97.7	20.0	171.1957	74.9295	0.417
209	GB6 B1121+7511	mps	-0.47	3.49	0.76	0.3	-0.39	0.07	4850	55.9	11.0	171.1946	74.9233	1.8
209	BWE 1121+7511	mps	-0.47	3.49	0.76	0.3	-0.39	0.07	4850	71.0	14.0	171.2021	74.9131	2.3
209	NVSS J112449+745531	mps	-0.4	3.23	0.76	0.3	-0.39	0.07	1400	100.0	20.0	171.2067	74.9254	0.75
235	WN B0838.7+7240	conc	0.39	1.76	0.3	0.24	-0.65	0.06	325	528.0	110.0	130.9951	72.499	0.2
235	MY 083841.1+723005.9	conc	0.39	1.76	0.3	0.24	-0.65	0.06	232	480.0	96.0	130.9888	72.5016	2.5
235	6C 083835+724058	conc	0.39	1.76	0.3	0.24	-0.65	0.06	151	410.0	82.0	130.9671	72.5028	4.2
235	7C 083842.00+724032.00	conc	0.39	1.76	0.3	0.24	-0.65	0.06	151	477.0	95.0	130.9921	72.4953	1.17
235	WSTBa 76W0443	conc	0.39	1.76	0.3	0.24	-0.65	0.06	327	557.0	110.0	130.996	72.4991	1.5
235	TGSSADR J084358.7+722956	conc	0.39	1.76	0.3	0.24	-0.65	0.06	150	405.0	81.0	130.9946	72.499	0.417
235	GB6 B0838+7240	conc	-0.69	4.48	0.3	0.24	-0.65	0.06	4850	99.0	20.0	130.9975	72.4964	1.8
235	87GB 083841.5+724036	conc	-0.69	4.48	0.3	0.24	-0.65	0.06	4850	116.0	23.0	130.99	72.4967	2.3
235	BWE 0838+7240	conc	-0.69	4.48	0.3	0.24	-0.65	0.06	4850	99.0	20.0	130.9904	72.4961	2.3
235	NVSS J084359+722955	conc	-0.58	4.21	0.3	0.24	-0.65	0.06	1400	247.0	49.0	130.9958	72.4987	0.75
235	WB 0838+7240	conc	-0.62	4.28	0.3	0.24	-0.65	0.06	1400	204.0	41.0	130.9904	72.4961	2.0
235	CLASS J084358.9057+722956.127	conc	-0.69	4.48	0.3	0.24	-0.65	0.06	8400	54.7	11.0	130.9954	72.4989	0.0055
284	TXS 0450+711	conc	0.57	1.78	0.48	0.24	-0.56	0.06	365	1750.0	350.0	73.9272	71.2247	0.1
284	WN B0450.0+7108	conc	0.57	1.78	0.48	0.24	-0.56	0.06	325	1730.0	350.0	73.9262	71.2246	0.2
284	MY 045001.1+711327.1	conc	0.57	1.78	0.48	0.24	-0.56	0.06	232	1340.0	270.0	73.9271	71.2242	2.5
284	6C 045000+710849	conc	0.57	1.78	0.48	0.24	-0.56	0.06	151	1060.0	210.0	73.9258	71.2272	4.2
284	TGSSADR J045542.2+711329	conc	0.57	1.78	0.48	0.24	-0.56	0.06	150	1290.0	260.0	73.926	71.225	0.417
284	GB6 B0450+7108	conc	-0.53	4.61	0.48	0.24	-0.56	0.06	4850	441.0	88.0	73.9246	71.2261	1.8
284	87GB 045000.3+710845	conc	-0.54	4.64	0.48	0.24	-0.56	0.06	4850	429.0	86.0	73.9237	71.2261	2.3
284	BWE 0450+7108	conc	-0.55	4.64	0.48	0.24	-0.56	0.06	4850	427.0	85.0	73.9246	71.2264	2.3
284	NVSS J045542+711328	conc	-0.54	4.64	0.48	0.24	-0.56	0.06	1400	938.0	190.0	73.9263	71.2245	0.75
284	WB 0450+7108	conc	-0.55	4.64	0.48	0.24	-0.56	0.06	1400	967.0	190.0	73.9246	71.2264	2.0
284	CLASS J045542.2916+711328.236	conc	-0.54	4.64	0.48	0.24	-0.56	0.06	8400	263.0	53.0	73.9262	71.2245	0.0055
287	TXS 0436+709	mps	1.02	-0.04	1.06	0.29	-0.76	0.07	365	387.0	77.0	70.4023	71.014	0.1
287	WN B0436.0+7055	mps	1.02	-0.04	1.06	0.29	-0.76	0.07	325	354.0	71.0	70.4002	71.0138	0.2
287	MY 043557.5+710117.0	mps	0.91	0.19	1.06	0.29	-0.76	0.07	232	160.0	53.0	70.3871	71.0214	2.5
287	MY 043608.4+710042.5	mps	1.02	-0.04	1.06	0.29	-0.76	0.07	232	240.0	52.0	70.4325	71.0118	2.5
287	TGSSADR J044136.5+710049	mps	1.02	-0.04	1.06	0.29	-0.76	0.07	150	156.0	31.0	70.4023	71.0137	0.417
287	GB6 B0436+7055	mps	-0.81	4.66	1.06	0.29	-0.76	0.07	4850	48.0	9.6	70.4029	71.0139	1.8
287	87GB 043559.0+705504	mps	-0.84	4.74	1.06	0.29	-0.76	0.07	4850	62.0	12.0	70.3929	71.0144	2.3
287	BWE 0435+7054	mps	-0.84	4.74	1.06	0.29	-0.76	0.07	4850	44.0	8.8	70.3958	71.0117	2.3
287	NVSS J044136+710049	mps	-0.71	4.4	1.06	0.29	-0.76	0.07	1400	168.0	34.0	70.4017	71.0138	0.75
287	WB 0435+7054	mps	-0.81	4.65	1.06	0.29	-0.76	0.07	1400	163.0	33.0	70.3958	71.0117	2.0
295	TXS 0358+703	mps	0.92	0.77	0.84	0.24	-0.69	0.08	365	1320.0	260.0	60.9357	70.448	0.1
295	WN B0358.4+7018	mps	0.92	0.77	0.84	0.24	-0.69	0.08	325	1080.0	220.0	60.9331	70.4479	0.2
295	6C 035827+701832	mps	0.92	0.77	0.84	0.24	-0.69	0.08	151	620.0	120.0	60.9333	70.4469	4.2
295	TGSSADR J040344.0+702652	mps	0.92	0.77	0.84	0.24	-0.69	0.08	150	582.0	120.0	60.9336	70.4479	0.417
295	GB6 B0358+7018	mps	-0.59	4.64	0.84	0.24	-0.69	0.08	4850	283.0	57.0	60.9308	70.4475	1.8
295	87GB 035826.3+701830	mps	-0.59	4.62	0.84	0.24	-0.69	0.08	4850	288.0	58.0	60.9279	70.4464	2.3
295	BWE 0358+7018	mps	-0.59	4.64	0.84	0.24	-0.69	0.08	4850	283.0	57.0	60.9292	70.4464	2.3
295	NVSS J040344+702653	mps	-0.59	4.62	0.84	0.24	-0.69	0.08	1400	760.0	150.0	60.9341	70.4481	0.75
295	WB 0358+7018	mps	-0.59	4.62	0.84	0.24	-0.69	0.08	1400	673.0	130.0	60.9292	70.4464	2.0
295	CLASS J040344.1955+702652.790	mps	-0.78	5.24	0.84	0.24	-0.69	0.08	8400	140.0	28.0	60.9341	70.448	0.0055
317	WN B0254.0+7216	mps	1.45	-1.05	1.43	0.37	-0.56	0.07	325	385.0	77.0	44.7567	72.4799	0.2
317	MY 025355.8+722929.6	mps	1.45	-1.05	1.43	0.37	-0.56	0.07	232	200.0	46.0	44.7338	72.4916	2.5
317	TGSSADR J025901.6+722846	mps	1.45	-1.05	1.43	0.37	-0.56	0.07	150	126.0	25.0	44.7569	72.4796	0.417
317	GB6 B0254+7216	mps	-0.54	3.94	1.43	0.37	-0.56	0.07	4850	108.0	22.0	44.755	72.4756	1.8
317	87GB 025402.4+721643	mps	-0.54	3.94	1.43	0.37	-0.56	0.07	4850	120.0	24.0	44.7608	72.4783	2.3
317	BWE 0254+7216	mps	-0.48	3.79	1.43	0.37	-0.56	0.07	4850	105.0	21.0	44.7596	72.4778	2.3
317	NVSS J025901+722843	mps	-0.66	4.43	1.43	0.37	-0.56	0.07	1400	297.0	59.0	44.756	72.4788	0.75
317	WB 0254+7216	mps	-0.66	4.43	1.43	0.37	-0.56	0.07	1400	290.0	58.0	44.7596	72.4778	2.0
317	CLASS J025901.3853+722844.387	mps	-0.54	3.94	1.43	0.37	-0.56	0.07	8400	66.9	13.0	44.7558	72.479	0.0055

Columns: Same designations as in Table B.1.

Table B.3: Total number of sources of all SPECFIND V3.0 catalogs in different frequency intervals.

Frequency	total number of sources ($\times 10^6$)
16.7 MHz $\leq \nu <$1.4 GHz	2,26
ν=1.4 GHz	2,83
1.4 GHz $< \nu \leq$ 31 GHz	0.40
16.7 MHz $\leq \nu <$325 MHz	1,52
ν=325 MHz	0,34
325 MHz $< \nu \leq$ 31 GHz	3,63

Appendix B.3: Uneven numbers of sources in both samples

We find roughly 6 times more sources with a spectral break around 325 MHz (18 075 sources) than sources with a break around 1.4 GHz (3104 sources). To investigate this difference in source numbers, we revisit the conditions that need to be fulfilled to identify spectral break sources via SPECFIND:

- the selection frequency point, either 325 MHz or 1.4 GHz, is included in both subsample spectra of the source.
- additionally to the selection frequency point, two independent frequency points must be found at each side of the peak frequency, which means each subsample has to contain three frequency points.

Thus, to find a spectral break source, we need to find at least five different flux density measurements, which means five different catalog tables in total. To evaluate possible biases, we consider Fig. 2. Even though we have a similar number of catalog tables at frequencies above and below 1.4 GHz, the low-frequency catalog tables cover a large fraction of the sky and contain a large number of sources. To show this quantitatively, Table B.3 presents the total number of sources for six different frequency bins. There are roughly six times more sources at frequencies smaller than 1.4 GHz than at higher frequencies. This trend is different for the frequency cut at 325 MHz: the number of sources at frequencies higher than 325 MHz is twice as high as the number of sources at frequencies lower than 325 MHz. Therefore, for the frequency cut of the catalogs at 1.4 GHz, the probability is much higher (nine times more sources) to find a corresponding high-frequency data point than to find a low-frequency data point. This unequal number is probably the reason for a smaller total number of spectral break sources. At the frequency cut at 325 MHz, the probability to find a low-frequency data point is only slightly smaller (2/3 times the sources number) than to find a high-frequency data point. This is probably the reason for the many more spectral break sources around 325 MHz.

Appendix B.4: Biases, false positive detections and number of compact sources - Comparison to other PS source samples

There are many studies about spectral break sources, providing new catalogs of candidates or confirming the spectral classification. This is done using new and/or existing public catalogs, like the WENSS catalog (Snellen et al. 1998) or by observing a sample of candidates at multiple frequencies. A recent study finds 261 GPS sources with frequency turnovers between 841 MHz and 1.4 GHz and additionally 1222 spectral break sources with turnover frequencies between 72 and 944 MHz within the GLEAM catalog (Callingham et al. 2017). These authors determined $\alpha_{\rm low}$ and $\alpha_{\rm high}$ by fitting a power law (i) to the 20 GLEAM flux densities and (ii) to the SUMSS and/or NVSS flux density point(s) together with the two central GLEAM flux density points (at 189 MHz and 212 MHz). They classified objects with $\alpha_{\rm low} \geq 0.1$ and $\alpha_{\rm high} > 0.1$ as GPS sources. In another recent study, Sotnikova et al. (2019) found 164 GPS sources based on observations of the candidate sample from Mingaliev et al. (2013).

We compared our results to these two recent studies, by first creating a combined sample of our two spectral break samples. With 18 075 spectral break sources around 325 MHz and 3104 around 1.4 GHz, we performed an internal cross-match and found 1310 sources that are included in both samples. This means that the peak frequency is not well defined for a significant number of GPS/MPS source candidates. The total number of unique spectral break source candidates is 19 869. To compare these sources with the Callingham et al. (2017) sample, we determined the amount of GLEAM sources in our sample. A sum of 9611 GLEAM sources is present in our combined sample around 1.4 GHz and 325 MHz. Comparing these GLEAM sources to the 1483 sources of the combined spectral break and GPS samples of Callingham et al. (2017), we found 697 matching sources (47%). Compared to their 261 GPS sources, we found 117 sources (45%) in our combined sample. From these 117 sources, 49 are classified by us as GPS/MPS sources and 11 as concave spectrum sources (51 %).

To investigate the relatively low number of matches and similar classifications, we inspected 50 Callingham et al. (2017) GPS sources by eye. We found 44% of the sources in our sample. Within these sources we have 50% matching classifications. The main reasons for the differences are

- SPECFIND missed 10% of the objects
- SPECFIND ignored a flux density measurement
- there were not enough flux density measurements at independent frequencies
- the peak flux was located above 3 GHz
- objects were HFP sources with positive spectral slopes

SPECFIND missed GPS sources because for frequencies below 500 MHz the only flux density measurement comes from GLEAM[10] and either there are less than three flux density measurements at independent frequencies above 500 MHz or there are three measurements that could not be fitted by a power law.

The percentage of common sources between our 325/1400 MHz break sample and the sample of Callingham et al. (2017) is caused by the fact that SPECFIND needs at least 5 flux density measurements at independent frequencies together with inhomogeneous coverages and sensitivities of the input catalogs. We call this effect the catalog selection bias. Within the sample of common sources, a similar classification is found for $\sim$ 40% of the sources. We call this the PS classification bias.

We analyzed possible false positive detections within our common GPS/MPS sample by investigating sources of our sample, which are present in the GLEAM catalog but not present in the Callingham et al. (2017) PS samples: 173 MPS and 30 GPS source candidates. Of these, 50 MPS and 30 GPS source candidates were inspected by eye using Aladin lite and the VizieR photometric viewer. In some cases the distance between the GLEAM position and those of the other surveys is larger than 10" but smaller than 20". Based on the NVSS images and the

[10] GLEAM has 20 independent flux density measurements, but in this work we have chosen to only use the wideband (170-231 MHz) flux density.

Full	Seq	Name	N	a	b [mJy]	nu MHz	S(nu) mJy	e_ mJy	RAJ2000 deg	DEJ2000 deg	SED	Radio+Opt	beam arcsec
1	339592	SUMSS J003356-452051	4	-0.90	5.41	843	5.92e+02	1.2e+02	008.4839	-45.3477	SED	view with aladin	18.00000
2	339592	PMN J0033-4521	4	-0.90	5.41	4850	9.50e+01	1.9e+01	008.4863	-45.3503	SED	view with aladin	168.00000
3	339592	PKS J0033-4520	4	-0.90	5.41	2700	2.10e+02	4.2e+01	008.4838	-45.3425	SED	view with aladin	60.00000
4	339592	MRC 0031-456	4	-0.90	5.41	408	1.14e+03	2.3e+02	008.4846	-45.3467	SED	view with aladin	120.00000
5	339591	WN B0010.0+4647A	4	0.40	0.63	325	4.30e+01	8.6e+00	003.1235	+47.0769	SED	view with aladin	12.00000
6	339591	GB6 B0009+4647	4	0.40	0.63	4850	1.18e+02	2.4e+01	003.1429	+47.0733	SED	view with aladin	108.00000
7	339591	CLASS J001229.2990+470434.698	4	0.40	0.63	8400	1.83e+02	3.7e+01	003.1220	+47.0763	SED	view with aladin	0.33000
8	339591	87GB 000956.0+464739	4	0.40	0.63	4850	1.23e+02	2.5e+01	003.1387	+47.0722	SED	view with aladin	138.00000
9	339590	WISH B2345.8-1852B	3	-0.89	4.51	325	1.54e+02	3.1e+01	357.1305	-18.6025	SED	view with aladin	18.00000
10	339590	VLSSr J234829.4-183539	3	-0.89	4.51	73	8.10e+02	1.6e+02	357.1229	-18.5943	SED	view with aladin	75.00000

Fig. B.6: The first ten entries of the VizieR table "spectra" within the SPECFIND V3.0 catalog.

source positions we think that our cross-identifactions are correct.

Moreover, we found that out of 300 MPS and 47 GPS source candidates that have a GLEAM frequency measurement in our samples, in total 108 (out of 300) MPS source candidates and 33 (out of 47) GPS source candidates do not have assigned a spectral index in the GLEAM catalog (Hurley-Walker et al. 2017b). An inspection of our MPS and GPS source candidates, which are absent in the Callingham et al. (2017) PS samples and have a GLEAM spectral index $\alpha > 0.1$, by eye did not show obvious classification problems. Callingham et al. (2017) derived their own spectral indices and could determine them for 96698 unresolved GLEAM sources with $\delta \geq -80°$ and $S_{200\mathrm{MHz,wide}} \geq 0.16$ Jy instead of 95568 sources with spectral indices selected by the same criteria in the GLEAM catalog. Based on these numbers we do not expect that many of the cross-identified GLEAM sources without a spectral index from the GLEAM catalog possess a spectral index derived by Callingham et al. (2017). 27 out of 47 SPECFIND GPS candidate sources and 51 out of 303 SPECFIND MPS source candidates with a GLEAM flux density measurement have $S_{200\mathrm{MHz,wide}} \geq 0.16$ Jy and are thus not included in the Callingham et al. (2017) PS samples. The inspection by eye of 20 SPECFIND MPS source candidates with $S_{200\mathrm{MHz,wide}} \geq 0.16$ Jy, which are absent in the Callingham et al. (2017) PS samples, showed that seven sources have no corresponding spectral index and only eight sources show $\alpha \geq 0.1$, which is the condition to identify a PS source. An inspection of these eight sources with the VizieR photometric viewer did not show any classification problem. We conclude that the absence of many of our MPS and GPS source candidates in the Callingham et al. (2017) PS source samples is due to the selection criteria of Callingham et al. (2017) and our classification of most of our MPS and GPS sources is probably correct. Furthermore, about half of the potentially MPS sources, which are false positive have a flat GLEAM spectral index of $-0.3 < \alpha < 0.1$. These sources are probably variable flat spectrum sources, where the variability occurs at frequencies higher than 1 GHz as the sources J1258+2820 and J1616+4632 in Dallacasa & Orienti (2016). One of these sources is QSO B1102-24, classified as QSO and blazar at a redshift of $z = 1.66$. This radio continuum source is strongly variable at frequencies $\gtrsim 1$ GHz (Fig. B.7). We think that these sources can well be classified as PS sources. Based on the number of MPS/GPS sources that are absent in the Callingham et al. (2017) PS samples with $\alpha < -0.3$ we estimate the percentage of false positives to be $\lesssim 20\,\%$.

The 164 GPS sources from Sotnikova et al. (2019) have peak frequencies in the range of 200 MHz to 25 GHz. With 99 of these sources that have peak frequencies above 2 GHz, this sample is biased toward higher frequencies. Since we are mostly sensitive to turnover frequencies around the selection frequencies of

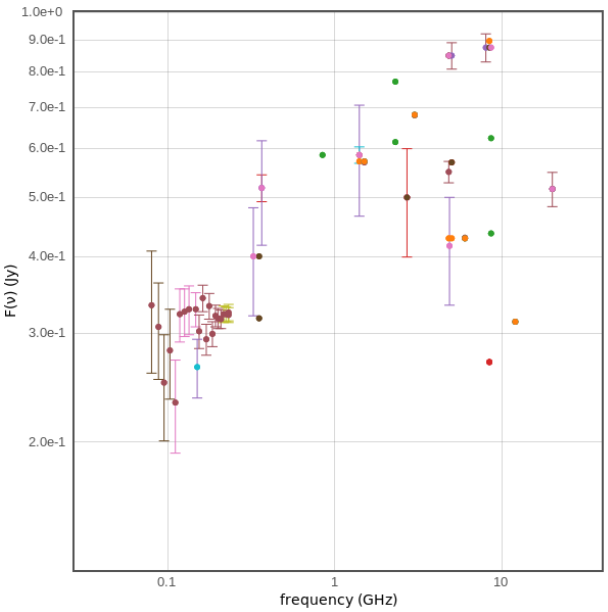

Fig. B.7: Radio SED of QSO B1102-24 established by the VizieR Photometry viewer. The source is strongly variable at frequencies $\gtrsim 1$ GHz.

325 MHz and 1.4 GHz, we compare to the 65 GPS sources with peak frequencies below 2 GHz and found 45 sources (69%) in our combined sample of 19 869 spectral break sources around 1.4 GHz and 325 MHz (catalog selection bias). We classified 21 sources (47%) as GPS/MPS/conc sources (PS classification bias).

We conclude from the comparisons with both studies from above that our PS source detection rate is about 50 % due to our catalog selection bias. In addition, our PS source classification rate among the PS source detections is about 50 %. We estimate the fraction of false positives in our sample of PS source candidates to be at maximum 20 %.

By investigating the peak frequencies of the overlapping sources from both studies from above, we can identify a turnover frequency range, where our method is most sensitive. In the 1.4 GHz sample, we find mainly spectral break sources with turnover frequencies around 1.4 ± 0.5 GHz. Additionally, sources were found that have turnover frequencies in the megahertz regime and in the higher-frequency regime (up to 15 GHz). In the 325 MHz sample we find mainly sources with turnover frequencies around 325 ± 175 MHz with additional sources found, which show turnover frequencies below 150 MHz and above 500 MHz.

Table B.4: Resolved sources in the FIRST14, CRATES, CLASS and TXS catalogs

	FIRST14	CRATES	CLASS	TXS	sum
GHz-break sources	644	683	926	1603	3856
resolved sources (GHz-break)	22	48	324	621	1015
resolved percentage	3%	7%	35%	39%	26%
GHz-PS sources	20	37	40	12	109
resolved sources (GHz-PS)	0	1	15	1	17
resolved percentage	0%	3%	38%	8%	16%
MHz-break sources	4535	1082	1089	16565	23 271
resolved sources (MHz-break)	486	116	378	8783	9763
resolved percentage	11%	11%	35%	53%	42%
MHz-PS sources	167	39	102	472	780
resolved sources (MHz-PS)	0	1	33	168	202
resolved percentage	0%	3%	32%	36%	26%

One defining feature of PS sources is that the majority of the sources are unresolved unless observations have milliarcsecond scale resolution (O'Dea & Saikia 2021). Due to our limited input catalog tables, we are not able to classify the sources based on their angular scale. Instead, we used the four catalogs with the highest resolution to investigate the compactness of the sources. To do so, we used the FIRST14, CRATES, CLASS and TXS catalogs with spatial resolutions $\leq 6''$. The criteria for unresolved sources are: FIRST14 - column fMaj<= 6", CRATES - column Morph=P; CLASS - column b/a=0; TXS - column Struct=P. The numbers of resolved sources are presented in Table B.4. Only two CRATES and no FIRST14 resolved PS-source candidates were found. Moreover, only one TXS PS-source candidate with a peak around 1 GHz is resolved. On the other hand, about 35 % of (i) the TXS PS-source candidates with a peak around 100 MHz and (ii) the CLASS PS-source candidates are resolved. Since the criteria in the CLASS and TXS catalogs are less stringent than those of the FIRST14 and CRATES catalogs, we decided to keep their PS classification. With the column "resolved," we flag sources in our online tables of spectral break source candidates. A conservative estimate of the resolved PS sources fraction is about 30 %.